HIghly advanced Probabilistic design and Enhanced Reliability methods for high-value, cost-efficient offshore WIND

Title: Physics-based component model validation

Deliverable no: D5.3

Delivery date: 30-09-2024

Lead beneficiary: DTU

Dissemination level: Public

This project has received funding from the European Union's Horizon 2020 Research and Innovation Program under Grant Agreement No. 101006689

Author information (alphabetical):		
Name	Organization	Email
Asger Bech Abrahamsen	DTU	asab@dtu.dk
Suguang Dou	EDF	suguang.dou@edfenergy.com
Abel Zeghidour	EDF	
Nassif Berrabah	EDF	nassif.berrabah@edfenergy.com
Clement Jacquet	EPRI	cjacquet@epri.com

Acknowledgements/Contributions::		
Name	Name	Name

Document information:					
Version	Date	Description	Prepared by	Reviewed by	Approved by
1.0	30.09.2024	Official	Authors listed above	N. Dimitrov	N. Dimitrov

Definition:	

Contents

List of Figures

1 Executive Summary

This deliverable report D5.3 is focused on validating the physics-based life model of the main bearing of SWT 2.3 - 93 m wind turbines installed in the Teesside wind farm operated in the United Kingdom by EDF. The bearing life model was originally developed as part of Hiperwind Deliverable 5.1 (Remigius et al., 2023). The following 3 issues have been identified during the Hiperwind project and the validation of these is central to this report:

1. The lifetime model of the FAG 230/800 main bearing of the SWT 2.3 - 93 turbine is based on the implementation of the ISO 281 standard for estimating the $L_{10} = \left(\frac{C}{P}\right)^a$ lifetime of roller bearings, where C is the capacity of the bearing, P is the equivalent bearing load and $a = 10/3$ is exponent for spherical roller bearings. The bearing loads P are estimated using the aeroelastic software Hawc2 in order to translate the wind environmental conditions characterized by the average wind speed v_{ave} and the reference turbulence intensity I_{ref}. However it is not known if the estimated loads are similar to the real loads of the wind turbines of the Teesside wind farms. Thus it is proposed to validate the thrust curve obtained from the Hawc2 code against the bending moment measured by strain gauges at the transition piece of the monopile of wind turbine no. 13.
2. One of the main challenges of using the ISO 281 standard to estimate the lifetime of main bearings of wind turbines is that the fluctuating wind will cause the temperature of the main bearing to fluctuate as well. This will affect the so-called modification factor for system approach a_{iso}, which must be multiplied onto the basic bearing lifetime L_10 in order to provide the modified lifetime of the main bearing, $L_{10m} = a_{iso} \cdot L_10$. Thus a validation of the prediction of the main bearing temperature as function of the wind speed is central in order to implement an a_{iso} correction of the lifetime obtained from the aeroelastic simulations.
3. A determination of the wind characteristics of the wind turbines of the Teesside wind farm in order to determine the input for the lifemodel. This validation has been included into the Hiperwind deliverable report D5.4 (Abrahamsen et al., 2024) and it is recommended that this is read in relation to the current report.
4. Finally, the predicted number of main bearing failures will be evaluated in comparison to the zero observed number of main bearing failures of the Teesside wind farm.

2 Introduction

The Hiperwind project has formulated a lifetime model of the FAG 230/800 main bearing of the SWT 2.3 - 93 turbines mounted in the Teesside wind farm, where the wind environmental conditions in terms of the annual average wind speed v_{ave} of the Rayleigh distribution and well as the reference turbulence intensity I_{ref} of the IEC normal turbulence model has been propagated to load using an aeroleastic model and evaluated into lifetime using the ISO 281 standard for roller bearings. This work is described in detail in the Hiperwind deliverable reports D5.1 and D5.4 (Remigius et al., 2023; Abrahamsen et al., 2024), which are recommended to be studied in relations to this report. Initial studies of the relation between the wind environmental conditions and the main bearing life indicated that "the lifetime of the main bearing was expected to increase as the reference turbulence intensity was increased." (See Hiperwind deliverable report D5.1).

This statement seems counter-intuitive to many wind turbine researchers, since the usual method of counting life of steel structures, like the turbine tower, is based on rainflow-counting of stress cycles and an SN-curve translating stress cycles into consumed life. When lifetime of bearings are estimated using the ISO 281 standard then the rainflow-counting method is replaced by a load level counting method, where the equivalent load of the bearing is evaluated in bins of revolutions, where the bearing is exposed to a constant load level. The main difference between the two methods is that the rainflow-counting is often not taking the mean load level into account and is only evaluating the stress cycle amplitudes. This is in contrast to the ISO 281 methods where the bearing load level is the main parameter evaluated in the lifetime estimation. Thus for the main bearing lifetime model the most important turbine load is the thrust force of the turbine rotor, because this is the main contribution to the axial load F_a of the main bearing. Since the radial load F_r of the main bearing is dominated by the weight of the turbine rotor, then this contribution can be considered as almost independent of the wind conditions and effectively the equivalent load of the main bearing appears as a scaled replicate of the turbine thrust curve (see Hiperwind deliverable D5.4 for an analysis of the aeroelastic simulations). From the above review of the important turbine loads feeding into the main bearing life model, it is obvious that a validation of the turbine thrust curve in comparison to the aeroelastic simulation is important.

The application of the ISO 281 standard of lifetime estimation of roller bearings includes the so-called modification factor of system approach a_{iso}, which must be multiplied onto the basic lifetime L_{10} in order to get the modified lifetime $L10m = a_{iso}L_{10}$. The system approach takes into account the cleanliness and temperature dependence of the kinematic viscosity of the grease used to lubricate the main bearing. The effect of a_{iso} is such that if the loads of the bearing are lower than the dynamic limit, then the lifetime is expected to increase exponentially and then "the bearing can practically run forever". The a_{iso} factor can, however, also decrease below 1, whereby the modified lifetime becomes considerably shorter than the basic lifetime L_{10}. This will be the case if the temperature of the main bearing is increasing too much and if the cleanliness of the grease changes from clean to dirty if debris particles accumulate during operation and the re-greasing system of the turbine is not supplying sufficient amounts of fresh grease to flush out the debris. Considerable effort has been done in the Hiperwind work package 5 in order to provide a simple model for estimating "a mean temperature" of the main bearing for the aeroelastic time-series simulation in order to evaluate the a_{iso} factor. The basic idea of the simple thermal model of the main bearing is that the friction heat dissipated inside the main bearing is conducted to the nacelle environment through the steel structures holding the main bearing and that the long term equilibrium temperature is obtained when heating power is equal to the cooling power. So the simple model neglects the heat capacity of all the steel surrounding the main bearing, and thereby does not consider the time delay between a change in dissipated power and the resulting temperature rise. However, for an average 10 minute time series at a specific wind speed in the aero-elastic simulation, it is not known what the previous history of the 10 min time series was. Under normal operation conditions one can assume that two adjacent 10-minute periods are quite similar. Thus the simple model averages out the wind speed fluctuations and provides a steady-state temperature. The validation of the assumptions behind the thermal model will be evaluated using the main bearing temperature time series of the SCADA data of the Teeside wind turbines. Another major question is if the main bearing lifetime model can be directly validated against the failure records of the Teesside wind farm. This is discussed as the last part of this report.

2.1 Teesside wind farm

The Teesside wind farm is located 1.5 km off the coast of the river Tees in the northern part of the United Kingdom(UK) near the city Middlesbrough, as illustrated in figure 2.1. The wind farm consists of 27 wind turbines mounted on monopiles at water depths ranging between 13-16 meters. The turbines are placed in 3 rows of 9 turbines each in a North-South heading. The wind farm started the operation in 2014 and is operated by EDF as of today.

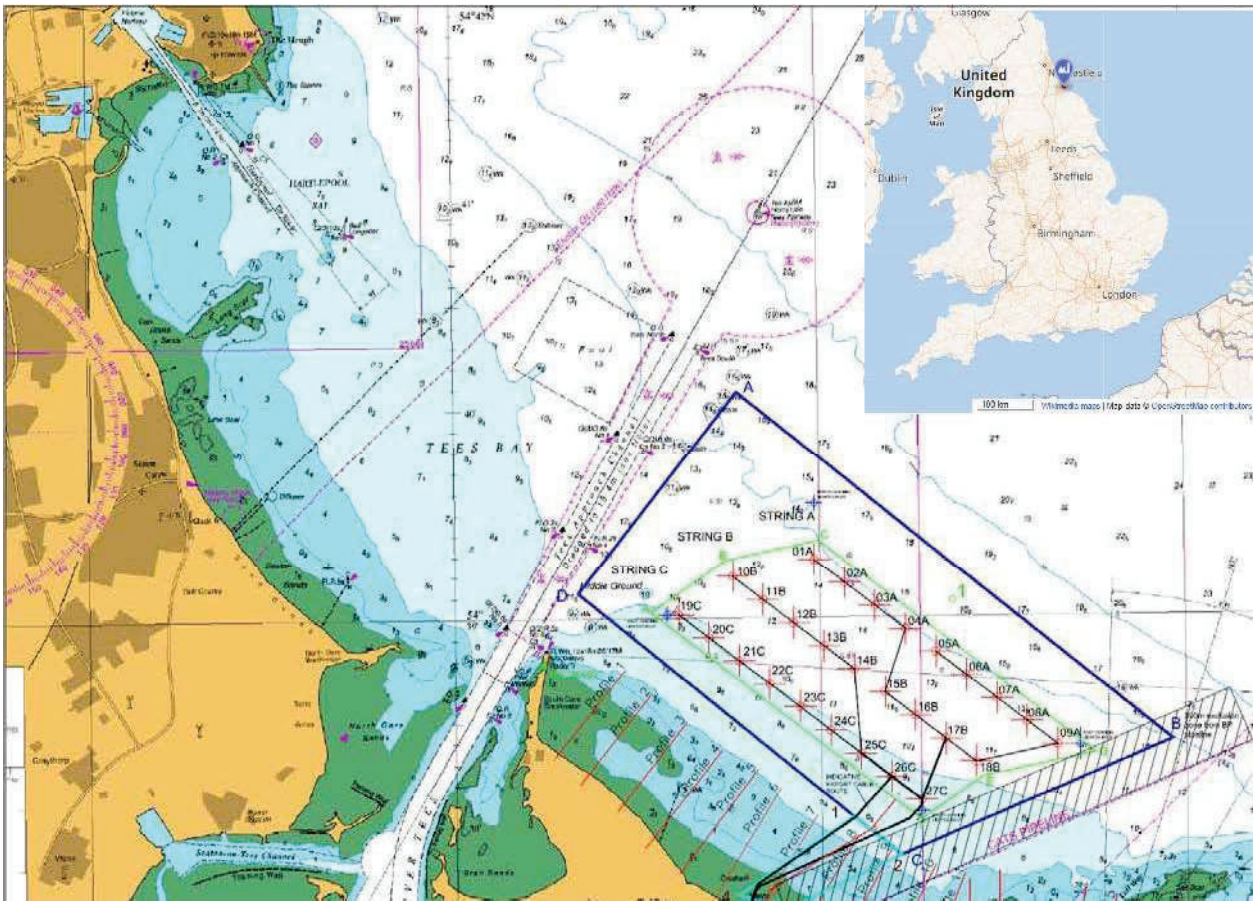

Figure 2.1: Illustration of layout of Teesside wind farm and the location is indicated in the inset. Reproduced from Bannister and McCall (2011)

2.2 SWT 2.3 MW - 93 m wind turbine

The Siemens Wind Turbine with the type specification SWT 2.3 MW - 93 m is a pitch regulated turbine with a rated power of 2.3 MW and a rotor diameter of 93 m. The drive train of the turbine consists of a 3-stage gearbox connected to a squirrel cage induction generator supported by a full power converter. This turbine model was introduced to the market in 2005 and has been installed in many offshore wind farms in Europe around 2010. In deliverable D5.1 more details on the drive train are provided and it is explained how the main bearing can be represented as a FAG 230/800 spherical double-row roller bearing as identified from spare part suppliers. Similarly, the grease used for the main bearing has been identified as Klüberplex BEM 41-301. An automatic re-greasing system will provide new grease for the main bearing from a grease cartridge mounted near the main bearing.

2.3 Instrumentation of the monopiles and turbines in Teeside

The SWT 2.3 - 93 turbines of the Teesside offshore wind farm provide 10 minutes average SCADA data of many operational parameters such as wind speed, wind direction, power production and temperatures of the main components of the drive train, such as the main bearing and gearbox. EDF collects the SCADA data in a database and a subset has been shared with the partners of Hiperwind. This dataset is used for the validation of the thermal model of the main bearing. Selected turbines of the Teesside wind farm have been instrumented with additional strain gauges on the transition piece of the monopiles, and measurements are collected at a frequency of 20 Hz. One month of strain gauge data of wind turbine WT13 has been shared in order to validate the thrust curve of the SWT 2.3 - 93 turbines.

3 Selection of validation cases and methodologies

The selection of the validation cases of the Hiperwind work package 5 is based on the measurements availability, as well as considerations of what validation information can be shared publicly. The original plan was to also include a physics-based life model of the bearings of the gearbox of the SWT 2.3 - 93 turbine, but early in the project is became evident that publicly shareable information about the PEAB 4456 gearbox could not be obtained. The focus of work package 5 was then put on the main bearing, because it was possible to identify representative bearings from public second-hand spare-part web sites as described in Hiperwind Deliverable 5.1 (Remigius et al., 2023). It is believed that the methodology of formulating a physics-based lifetime model of the main bearing of the SWT 2.3 - 93 turbine is somewhat similar to the formulation of the gearbox bearings, but the uncertainty of the gearbox specifications would make such an attempt unfeasible for the gearbox. It was however evident from discussions with EDF maintenance crew of the Teesside wind farm that gearbox replacements are ongoing, whereas no main bearings have been replaced yet. However, the cost of replacing a main bearing of the turbines at Teesside will need a jack-up vessel, and it is therefore considered relevant to investigate.

4 Results

4.1 Temperature dependence of the main bearing and the a_{iso} factor

The initial work on formulating a physics-based life model of the main bearing in Hiperwind deliverable D5.1 showed that the modified lifetime $L_{10m} = a_{iso}L_{10}$ of the bearing could be estimated if the so-called modification factor for system approach could be determined and then multiplied onto the basic bearing life L_{10} dictated purely by the bearing loads. The determination of the a_{iso} factor is described in the ISO 281 standard ISO281 (2007) and with additional information in the ISO 1281 technical report TR1281-2 (2009). More detailed notes are often provided by the bearing manufacturers and Schaeffler has published a technical note TPI 176, which has been applied to the FAG 230/800 main bearing covered by this report.

The main purpose of the a_{iso} factor is to quantify if the bearing loads P_{eq} are considerably lower than the fatigue limit load C_u of the bearing and if the bearing is expected to have almost infinite lifetime. One of the main parameters for evaluating the a_{iso} factor is the ratio

$$p_1 = \frac{e_C C_u}{P_{eq}} \tag{4.1}$$

where the life adjustment factor for contamination e_C of the Kluberplex 41-301 grease used to lubricate the FAG 230/800 bearing has been included. The life adjustment factor for contamination ranges between zero and one. It can be considered as an adjustment of the fatigue limit load C_u with $e_c = 1$ meaning clean grease and the bearing have the full fatigue limit load, whereas $e_c \to 0$ have heavily contaminated grease and a resulting fatigue limit load of the bearing approaching zero $e_c C_u \to 0$. The second important input parameter to the determination of the modification factor for system approach a_{iso} is the ratio of the grease kinematic viscosity ν and the reference viscosity ν_1, both at the operation temperature T of the bearing. This ratio is often denoted as the κ ratio of the grease

$$\kappa = \frac{\nu(T)}{\nu_1(T)} \tag{4.2}$$

The a_{iso} factor can be considered as a function of the p_1 parameter as well as the viscosity ratio κ and bearing manufacturers are often tabulating the resulting a_{iso} factor as illustrated in Figure 4.1 .

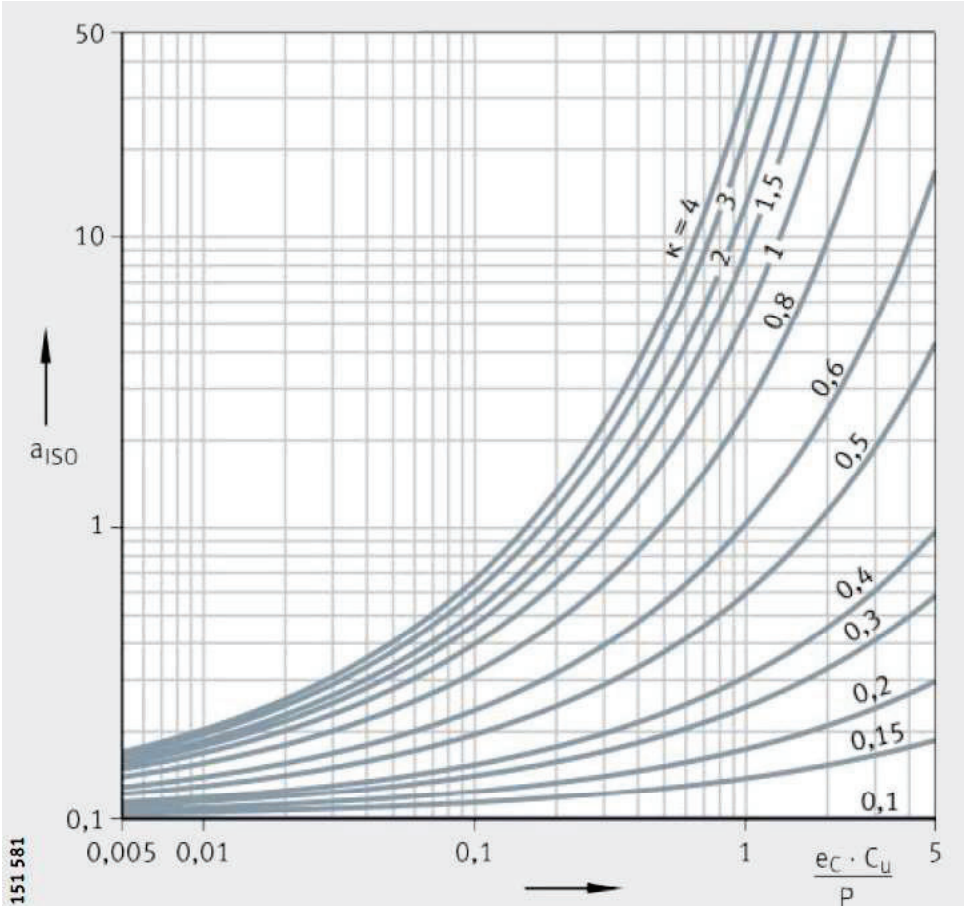

Figure 4.1: Illustration of the modification factor for system approach a_{iso} which must be multiplied onto the Basic bearing life L_{10} in order to obtain the modified bearing life $L_{10m} = a_{iso}L_{10}$. Reproduced from Schaeffler note TPI 176 Schaeffler (2013)

The determination of the viscosity ratio κ must be done for the operating temperature of the main bearing. This becomes a coupled problem, because the operating temperature is a function of the friction heating of the bearing, which by itself depends on the viscosity of the grease. Thus, a set of non-linear equations must be solved iteratively in order to obtain the operation point of a bearing once the load inputs are known. This method has already been described in Hiperwind deliverable D5.1 and the friction heating power Q_B will be shown without any constants:

$$Q_B \approx (M_0 + M_1)\, n \approx \left(M_0 + \left(\frac{F_r + 3Fa}{C_0}\right)^{0.5}\right) n \tag{4.3}$$

where M_0 is the frictional torque as function of speed, M_1 is the frictional torque as function of load, n is the rotation speed of the bearing, F_r is the radial load of the bearing, F_a is the axial load of the bearing, C_0 is the Basic static load rating of the bearing. The term M_0 can be considered as constant and it is therefore interesting to examine the influence of the radial F_r and the axial F_a loads.

Both Hiperwind deliverables D5.1 and D5.4 found that the radial load of the bearing F_r can be considered as independent of the turbine wind speed, since it is dominated by the weight of the turbine rotor resting on the main bearing. The axial load F_a on the other hand was found to

be almost a replicate of the turbine thrust curve. Thus it is seen from eq.(4.3) that the friction power dissipated in the main bearing is expected to scale with the square root of the thrust force F_a multiplied by the rotation speed n of the turbine. These two parameters can be computed from the aeroelastic simulation and one should therefore be able to provide an estimate of the operating conditions of the main bearing as part of the aeroelastic simulations.

Once the friction heating power Q_B has been determined, one can solve for the temperature increase ΔT above the ambient temperature according to

$$Q_B = k_q A_r \Delta T \Rightarrow \Delta T = \frac{Q_B}{k_q A_r} \tag{4.4}$$

where k_q is the heat transfer coeffiecient through the material surrounding the bearing and A_r is the surface area of the bearing through which the heat is transferred to the ambient surroundings.

Thus the simple thermal model above suggests that the temperature increase of the main bearing is scaling directly with the friction heating power, which is expected to be the product between the thrust force and the turbine rotation speed.

4.1.1 Thermal path of main bearing support

In order to implement the main bearing thermal model of Hiperwind deliverable D5.1 then the path of conducting the heat away from the main bearing of the SWT 2.3 - 93 turbine had to be specified. Figure 4.2 is showing how the main bearing and the main shaft of the turbine looks and Figure 4.3 is illustrating the corresponding thermal paths going through the main shaft and the support of the main bearing.

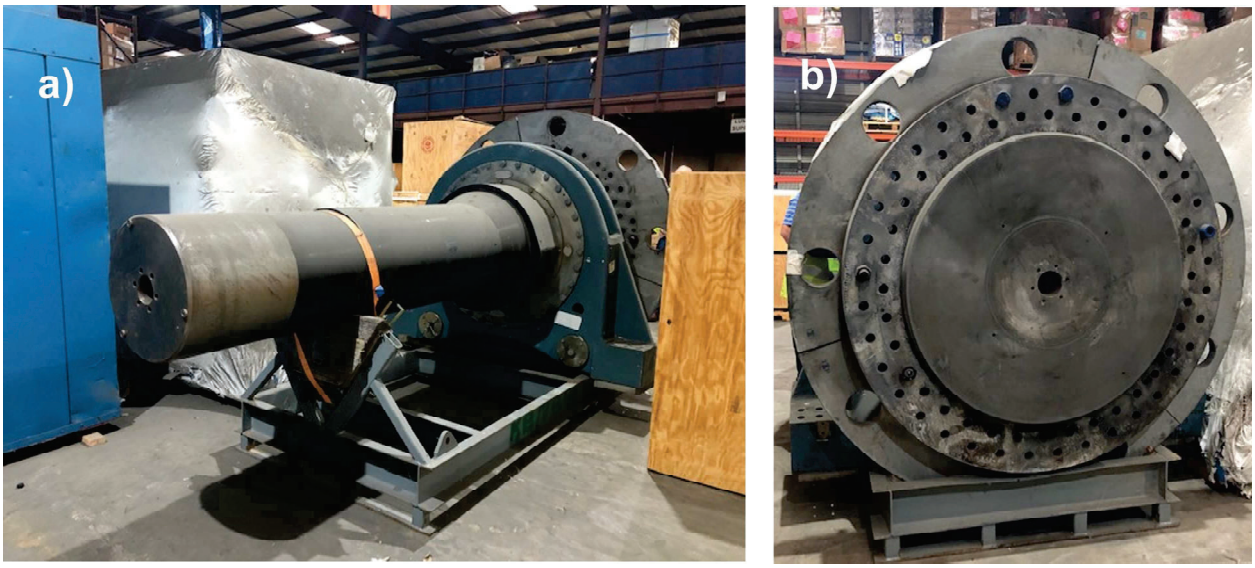

Figure 4.2: Picture of a main shaft and main bearing of a SWT2.3 - 93 turbine spare part as shown by the second-hand spare part trading company SparesInMotion. a) Main shaft seen from the position of the gearbox. b) Main bearing flange for holding the hub of the rotor as seen from the Hub side.

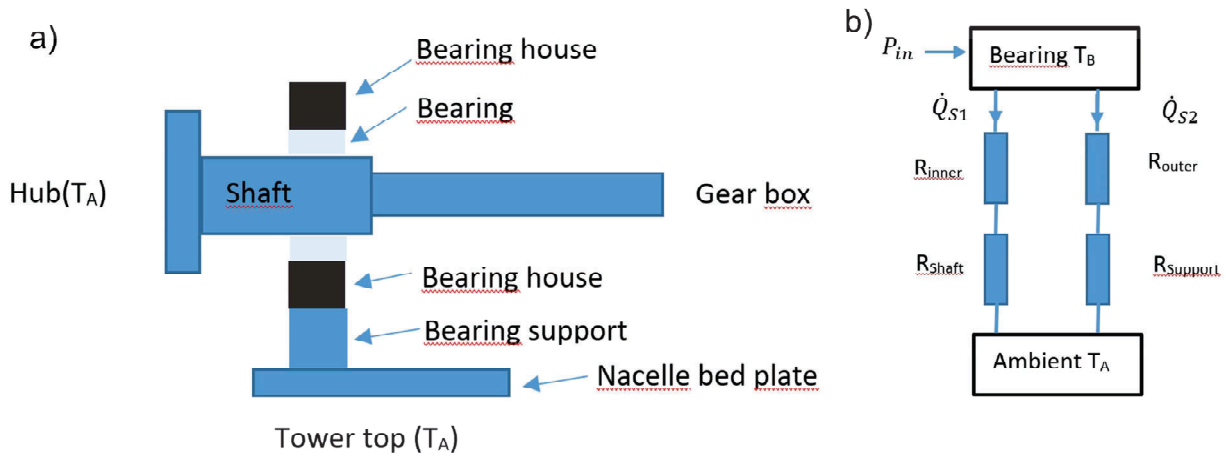

Figure 4.3: Illustration of the simple thermal model of the main bearing support of the SWT2.3 - 93 turbine. a) Cross section geometry of the main shaft and main bearing. b) Thermal model showing that the friction heat of the main bearing P_{in} is dissipated through the main shaft and to the hub flange as well as through the main bearing support and to the nacelle bedplate. The hub and the bedplate are assumed to have a temperature equal to the ambient temperature of the turbine.

The resulting heat coefficient of the main bearing was estimated from the estimated dimensions of the shaft and bearing housing shown in Figure 4.2 and used when solving the equations for determining the a_iso as described in D5.1.

4.1.2 Teesside main bearing temperature measurements

SCADA data from year 2019 holding the temperatures of the drive train components of the SWT2.3 - 93 turbines has been analyzed and Figure 4.4 shows the variation of the ambient temperature of the turbine, the main bearing, the hydraulic oil of the pitch system and the gearbox temperature for turbine number WT01. The first observation to be noted from Figure 4.4 is that the seasonal variation of the ambient temperature has very little impact on the temperature of the drive train components. The reason for this is that a de-humidifier system is maintaining a reduced humidity and a minimum temperature inside the nacelle, because the SWT2.3- 93 turbines of Teesside are installed offshore. Additional heating systems are most likely also applied to the hydraulic oil circulation system, which controls the temperature of the hydraulic oil to be $T_{hydraulic} = 35^oC$ all year around. This heating strategy is most likely also applied to the gearbox, where a minimum temperature of $T_{gearbox,min} \approx 30^oC$ is maintained. The maximum temperature of the gearbox is most likely limited by circulating the gearbox oil to a cooling device. The temperature variation of the main bearings is also quite limited and is seen to be in the range of $T_{mb} = 20 - 45^oC$. The lower limit is most likely related to the de-humidifier system keeping the nacelle temperature higher than the ambient temperature. The upper limit of the main bearing is expected to be determined by the heat dissipated in the main bearing and the cooling power of the surroundings.

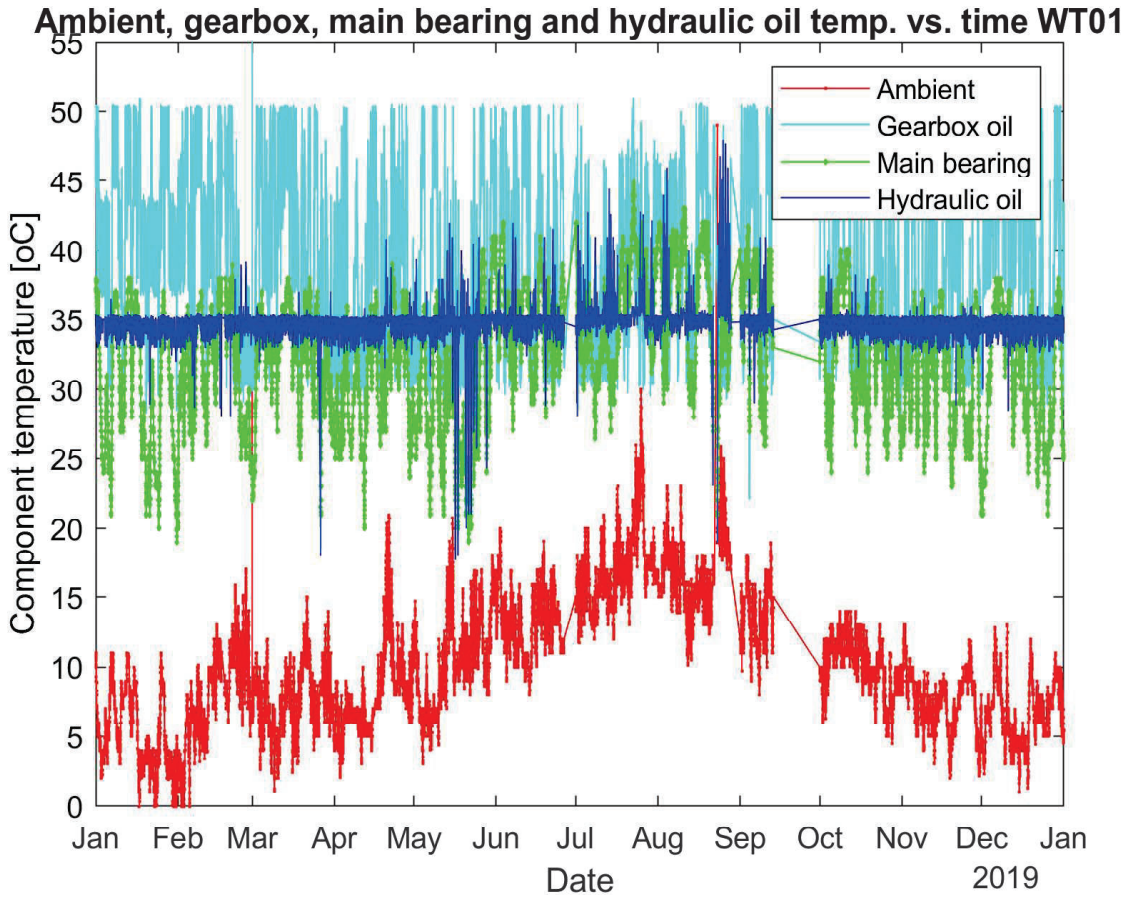

Figure 4.4: The annual temperature variation of selected drive train components of the WT01 turbine of Teesside wind farm in 2019. The ambient temperature outside the wind turbine is shown in red, the main bearing temperature in green, the temperature of the hydraulic oil in blue and the gearbox temperature in cyan.

Figure 4.5, Figure 4.6 and Figure 4.7 are showing the temperature variation of the drive train components of the 9 upper, the 9 middle and the 9 lower turbines of the Teesside wind farm in 2019. It is seen that the turbines behave quite similarly to WT01 as shown in Figure 4.4. All the turbines show a gap in the temperature SCADA data in September and a smaller gap in late June. The turbines Wt08 and WT12 show an almost 2 month gap from late June to start September and this is believed to be connected to maintenance of the drive trains of these turbines. There are a few incidents of the nacelle heating system being out of operation and for WT25 this can be observed around mid January, where the temperature of both the hydraulics and the main bearing is decreasing all the way down to the ambient temperature of $T_{amb,WT25,Jan} \approx 2^oC$.

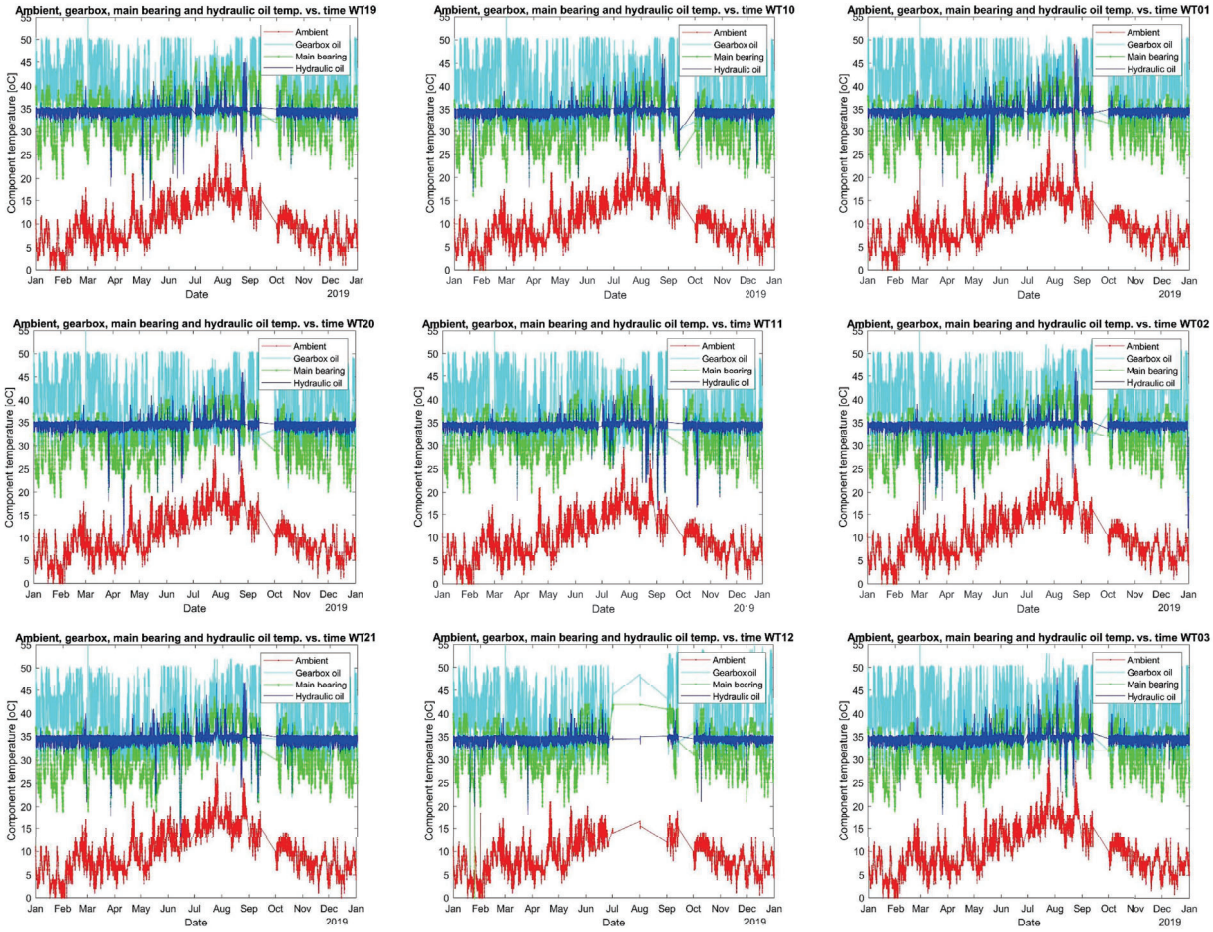

Figure 4.5: Overview of the drive train temperatures of the 9 upper turbines of the Teesside wind farm with the left column of turbines is facing land and the right column is facing the seaside as illustrated in Figure 2.1.

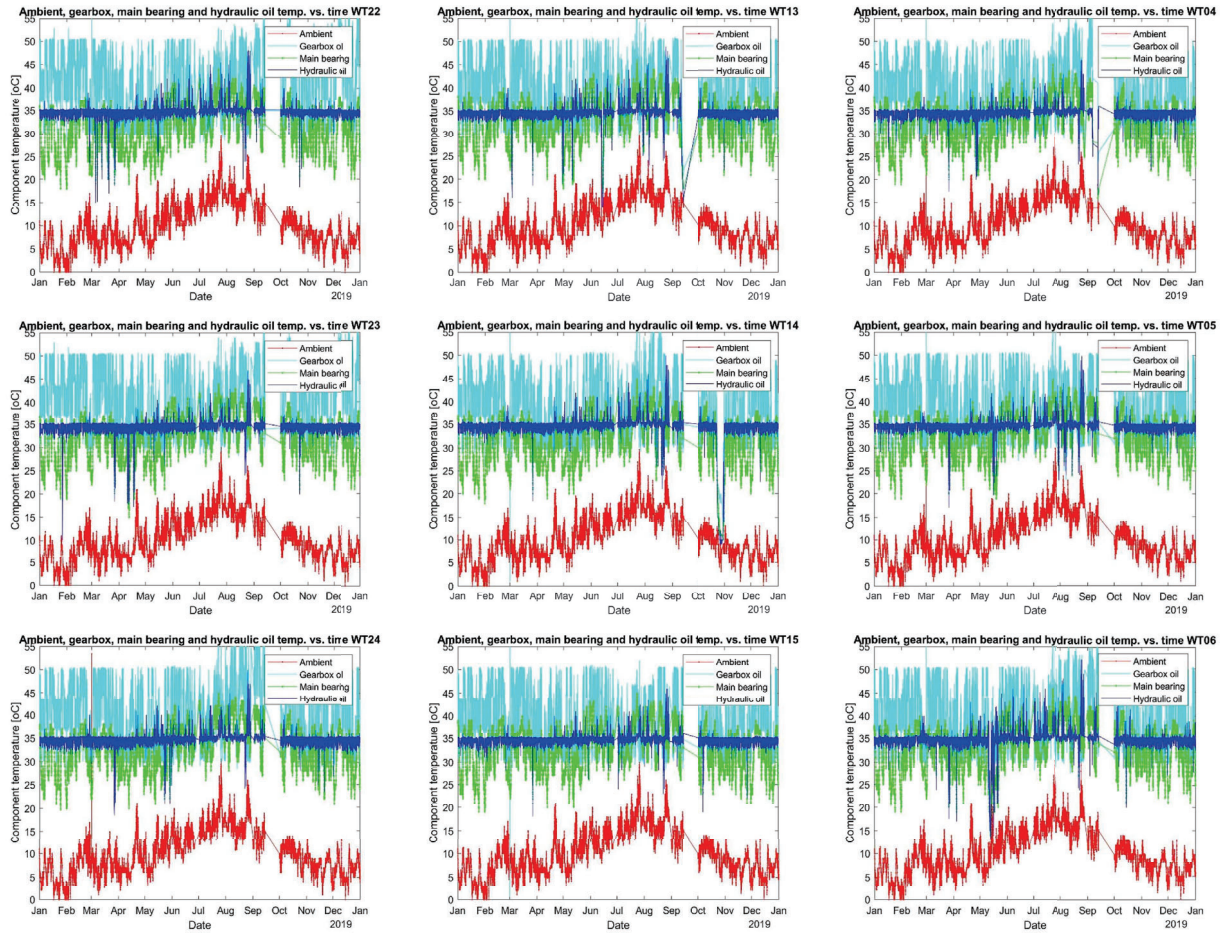

Figure 4.6: Overview of the drive train temperatures of the 9 middle turbines of the Teesside wind farm with the left column of turbines is facing land and the right column is facing the seaside as illustrated in Figure 2.1.

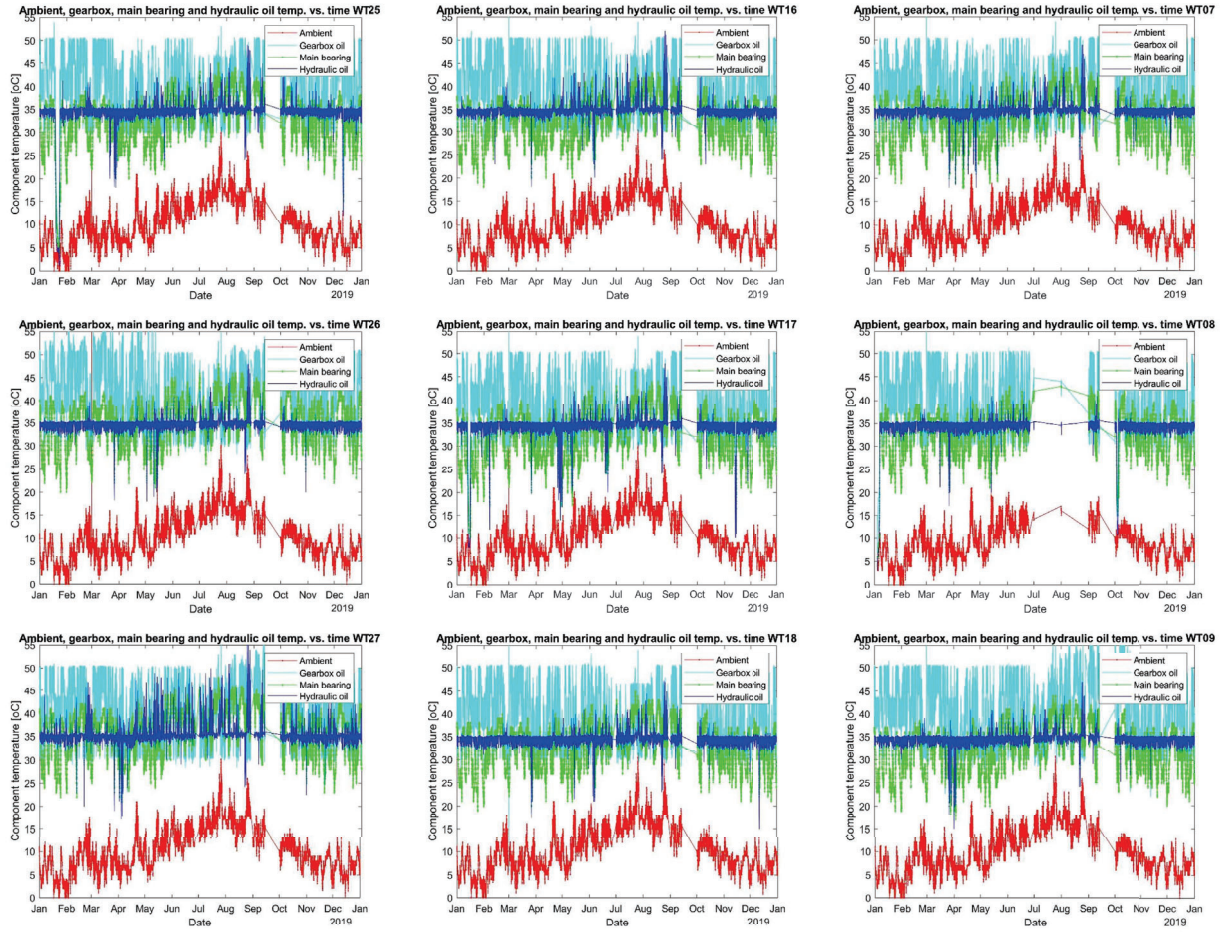

Figure 4.7: Overview of the drive train temperatures of the 9 lower turbines of the Teesside wind farm with the left column of turbines is facing land and the right column is facing the seaside as illustrated in Figure 2.1.

In order to illustrate the similarity of the main bearing temperatures of the 27 Teesside turbines then Figure 4.8 shows the main bearing temperature as well as the ambient temperature for all the turbines. A small seasonal effect with an average increase to the main bearing temperature in the order to 5^oC might be present between winter and summer, but this is considerably smaller than the variation of the ambient temperature in the order of 20 ^oC. Again this is believed to be caused by the de-humidifier system maintaining a nacelle temperature around 20^oC. Figure 4.9 shows the main bearing temperature of all 27 turbines in 2019 along with the wind speed of the turbines and this can be used to construct a cloud plot showing the correlation between the main bearing temperature and the wind speed as illustrated for the WT01 turbine in Figure 4.10. It can be seen that the temperature of the main bearing is measured with a resolution of 1 degree Celcius in the SCADA data and the 10 min average value is therefore often an integer if the temperature is not changing in the 10 min interval of the averaging. In the case of turbine WT01 it is seen that the main bearing temperatures are in the range between $T \approx 19 - 45^oC$ and the turbine is exposed to wind speeds up to $u = 25m/s$.

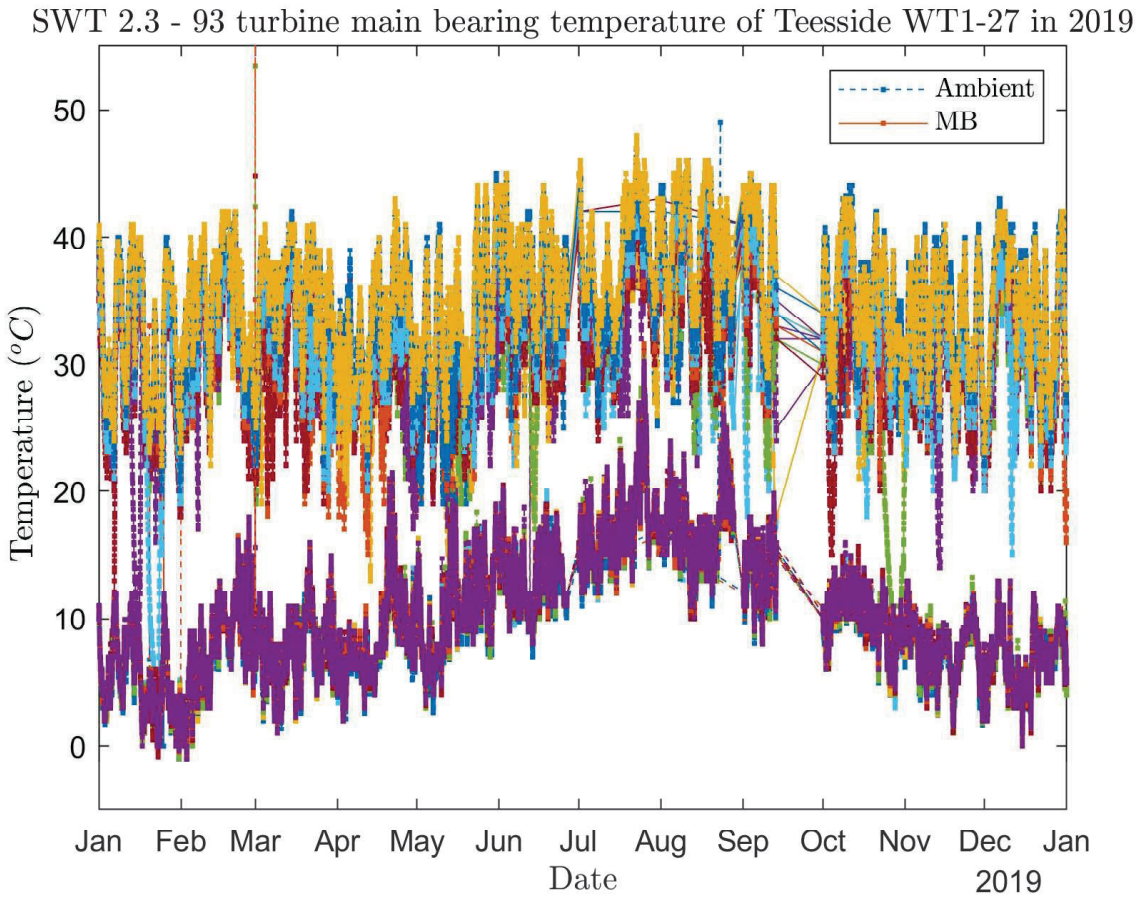

Figure 4.8: Temperature of the main bearings (MB) of the 27 Teesside SWT2.3 - 93 turbines in 2019 (top curves at 30 ^oC in January) along with the ambient temperature (Ambient at 5 ^oC in January) outside the turbines. A seasonal variation of the ambient temperature is clearly observed and this is also seen to be reflected in the main bearing temperature in the summer months (June-October).

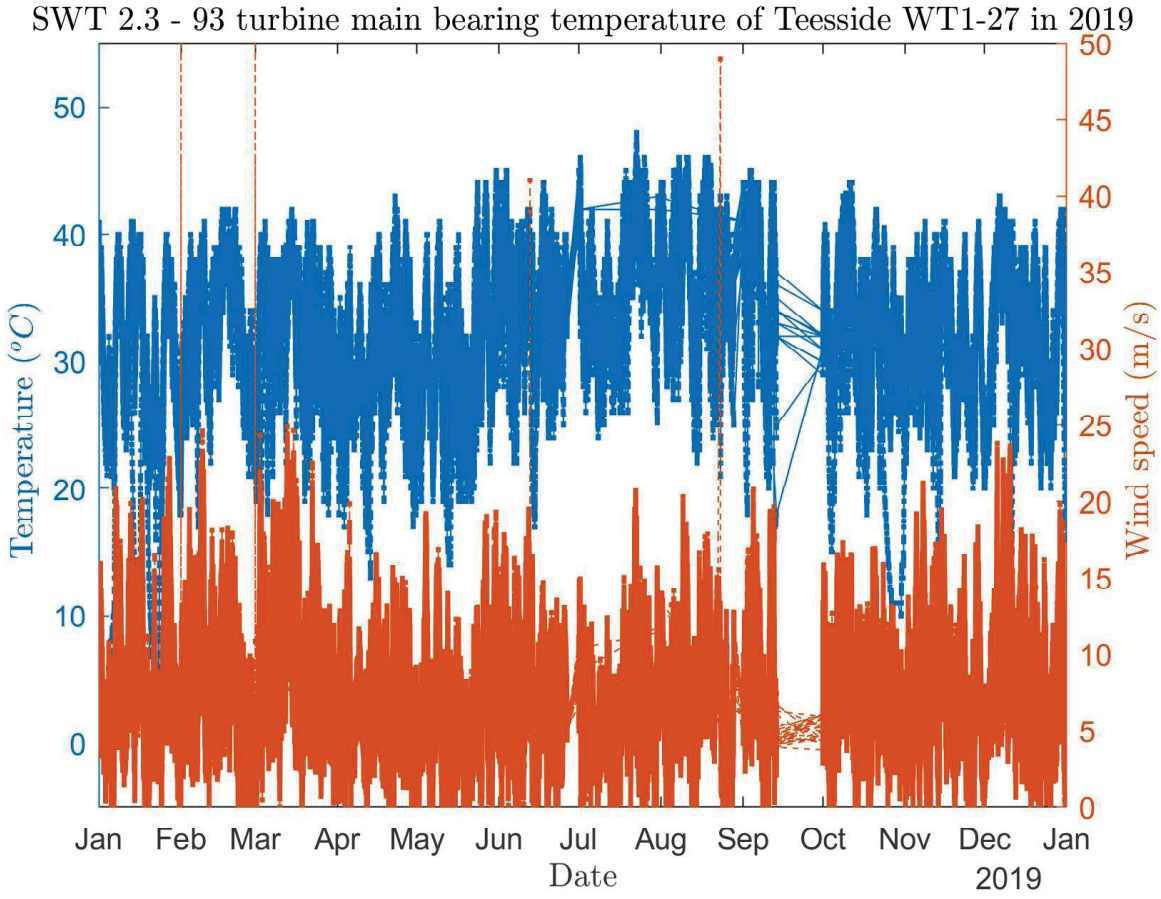

Figure 4.9: Temperature of the main bearings (MB) of the 27 Teesside SWT2.3 - 93 turbines in 2019 along with the wind speed (Ambient) outside the turbines. A seasonal variation of the ambient temperature is clearly observed and this also seen to be reflected in the main bearing temperature in the summer months (June-October).

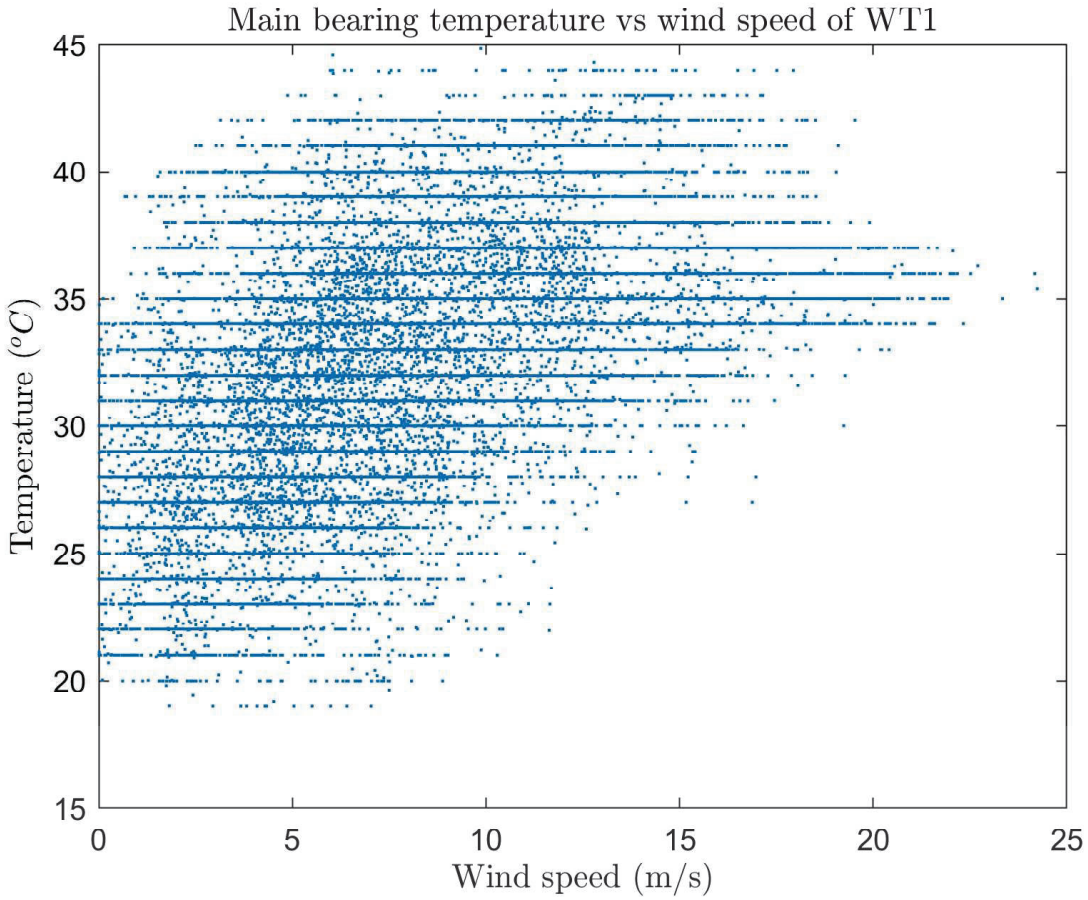

Figure 4.10: Cloud plot of the correlation between the main bearing temperature SCADA data and the wind speed of the WT01 turbine of the Teesside wind farm in 2019.

4.1.3 Comparison of main bearing temperature measurements with prediction from aeroelastic simulations

The measurements of the main bearing temperature shown as a function of the wind speed from the SCADA database of the Teesside wind farm can be compared with the dependence predicted from the aeroelastic simulations of the SWT 2.3 - 93 turbine as outlined in Hiperwind Deliverable D5.4. Figure 4.11 shows the predicted main bearing temperature as function of the wind speed u as well as the turbulence intensity TI obtained from Hawc2 simulations and the thermal equilibrium model discussed earlier.

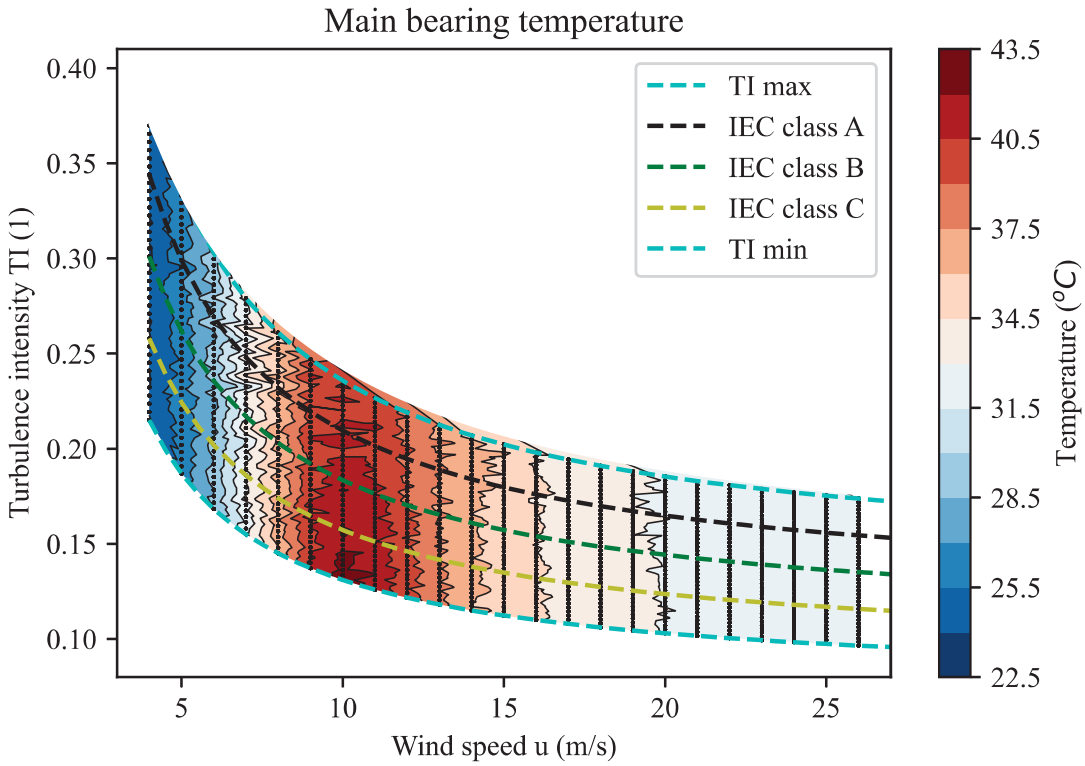

Figure 4.11: Predicted correlation between the main bearing temperature and the wind speed u and turbulence intensity TI of the SWT 2.3 - 93 turbine as obtained from aeroelastic simulations using the Hawc2 aeroelastic code. Reproduced from Hiperwind Deliverable report D5.4.

The cloud point plot of the correlation between the main bearing temperature and the wind speed as shown in Figure 4.10 can be difficult to compare to the results of Figure 4.11, therefore a two-dimensional density plot showing the probability of observing a certain main bearing temperature and wind speed in the measurements has been created. Figure 4.12 shows the probability density plot of the the main bearing temperature and the wind speed for the Teesside wind turbine WT01. The aeroelastic simulated dependence from Figure 4.11 has been added to the plot using dots for the different turbulence intensities in the range $I_{ref} = 0.10 - 0.18$ and open symbols for $I_{ref} = 0.14$, which is the approximate level of the Teesside wind turbines as determined in Hiperwind Deliverable D5.4.

It is observed that the simulations are covering the same temperature range as the measurements and that an increase of the main bearing temperature is seen from the cut-in wind speed at $u_{cut-in} = 4m/s$ and up to the rated wind speed at $u_rated \approx 11m/s$. The simulated correlation is expected to show a peak, but the measurements are showing a plateau for wind speeds above the rated wind speed. One should note however that the amount of data for wind speeds above 15m/s is quite limited, meaning the data-derived results for such wind speeds are uncertain.

Separate comparisons of the measured and simulated correlations are shown in Figure 4.13, 4.14 and 4.15 for the 9 upper, the 9 middle and the 9 lower turbines of the Teesside wind farm respetively. The general picture as outlined above is observed for most of the turbines, but some plots show a larger temperature scaled, because the humidity system failed to maintain the

heating of the nacelle like turbine WT25 in January.

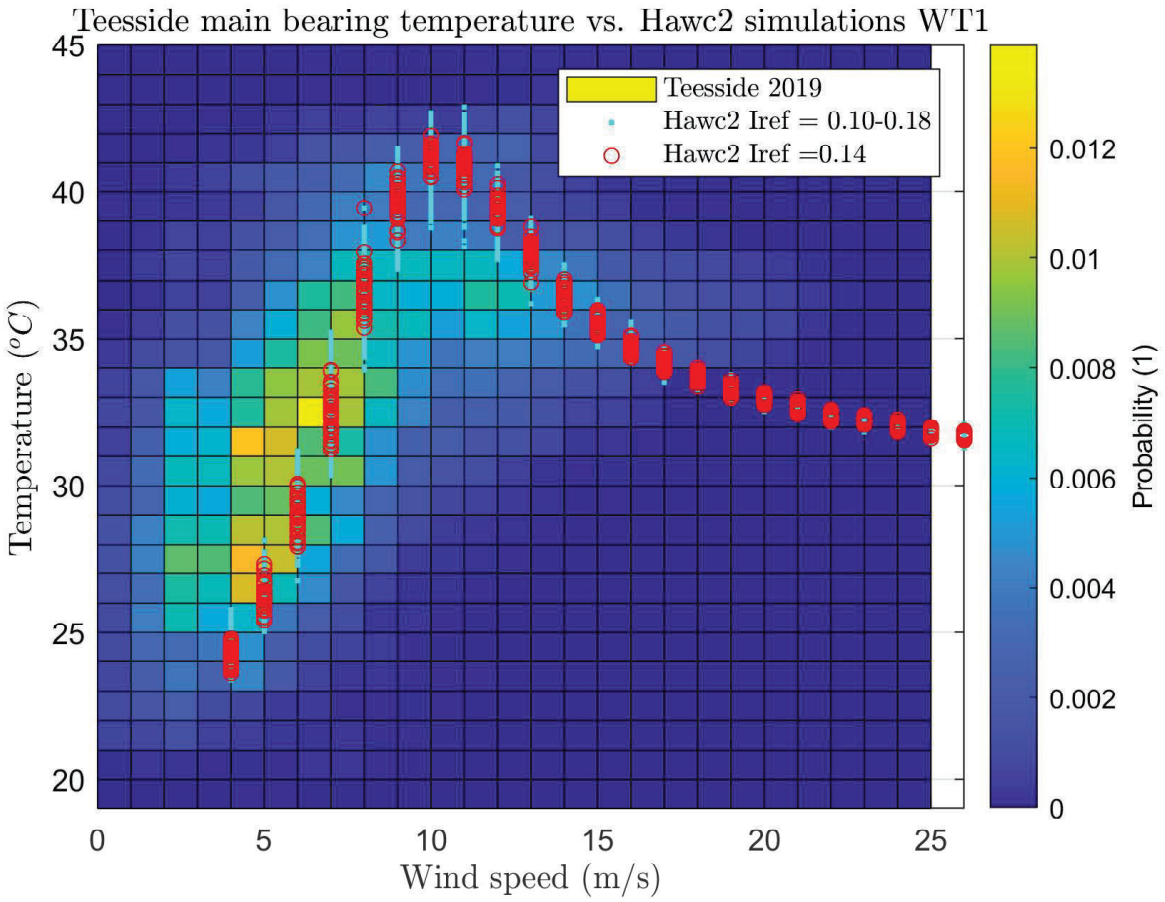

Figure 4.12: Comparison of the measured correlation between the main bearing temperature as a function of wind speed of the Teesside wind turbine WT01 in 2019 and the predicted correlation obtained from aeroelastic simulations in the Hiperwind Deliverable report D5.4. The color map shows the probability of observing a certain main bearing temperature at a given wind speed in the SCADA measurements of the Teesside wind turbine.

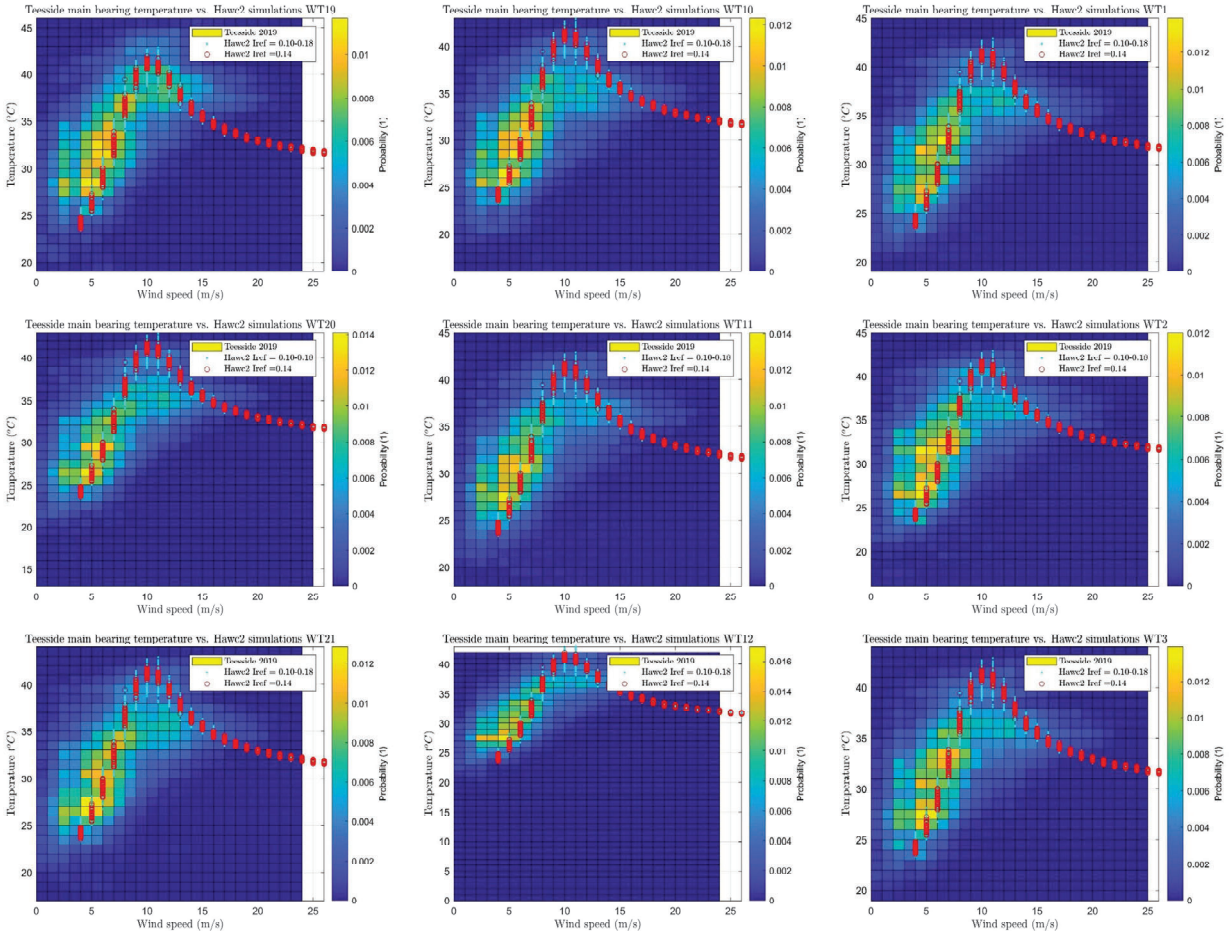

Figure 4.13: Overview of the correlation between the main bearing temperature and the wind speed of the measured SCADA data and the prediction of the aeroelastic simulations for the 9 upper turbines of the Teesside wind farm.

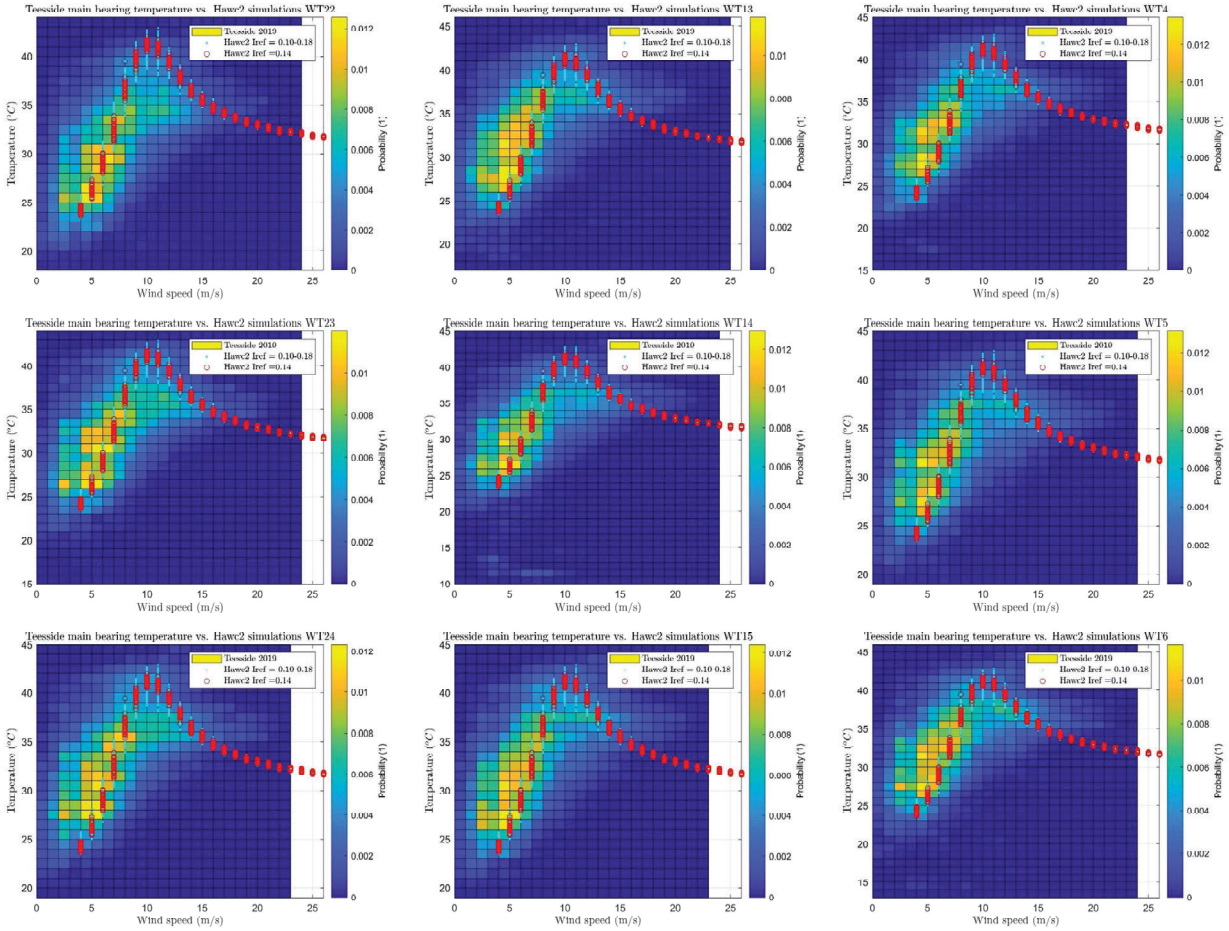

Figure 4.14: Overview of the correlation between the main bearing temperature and the wind speed of the measured SCADA data and the prediction of the aeroelastic simulations for the 9 middle turbines of the Teesside wind farm.

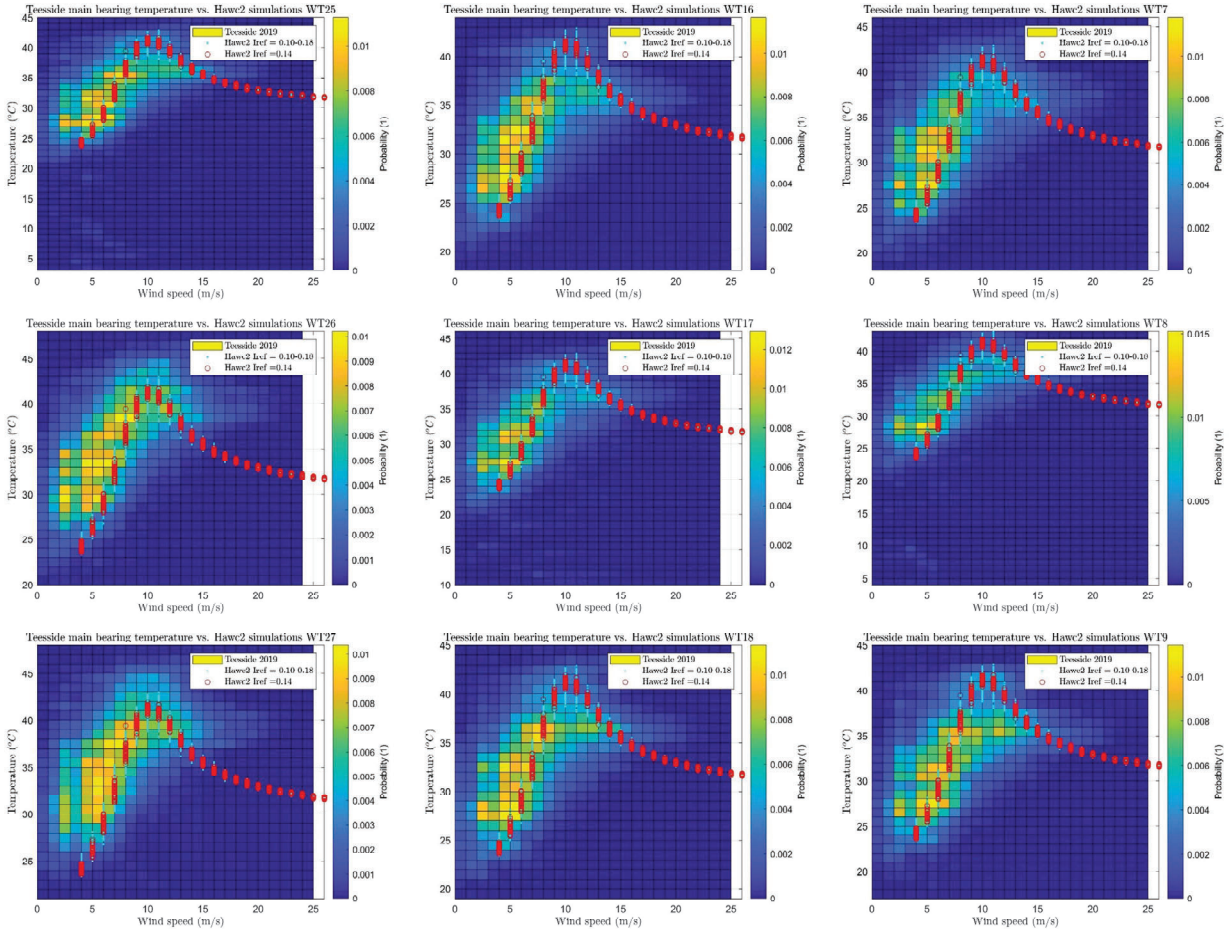

Figure 4.15: Overview of the correlation between the main bearing temperature and the wind speed of the measured SCADA data and the prediction of the aeroelastic simulations for the 9 lower turbines of the Teesside wind farm.

Finally, Figure 4.16 is showing the observed relationship between the wind speed and the main bearing temperature of all the 27 turbines of the Teesside wind farm, and the same dependence derived from the aeroelastic simulations. In general terms one can say that the predicted temperature range is very similar to the measured main bearing temperatures and that the increase from the cut-in wind speed and to the rated wind speed is reproduced. Above rated wind speed the measured main bearing temperature appears more constant and it does not appear as "peak-like" as the predicted correlations. Finally, the predicted relationship seem to match the lower bound of the measured main bearing temperatures around the cut-in wind speed, and also to be close to the upper bound of the measurements at the rated wind speed. The origin of this discrepancy will be discussed in the discussion section. It can however be concluded that the predicted relationships between the main bearing temperature and the wind speed describe the measured main bearing temperatures of the Teesside wind farm quite well and the model is thereby validated by the measurements.

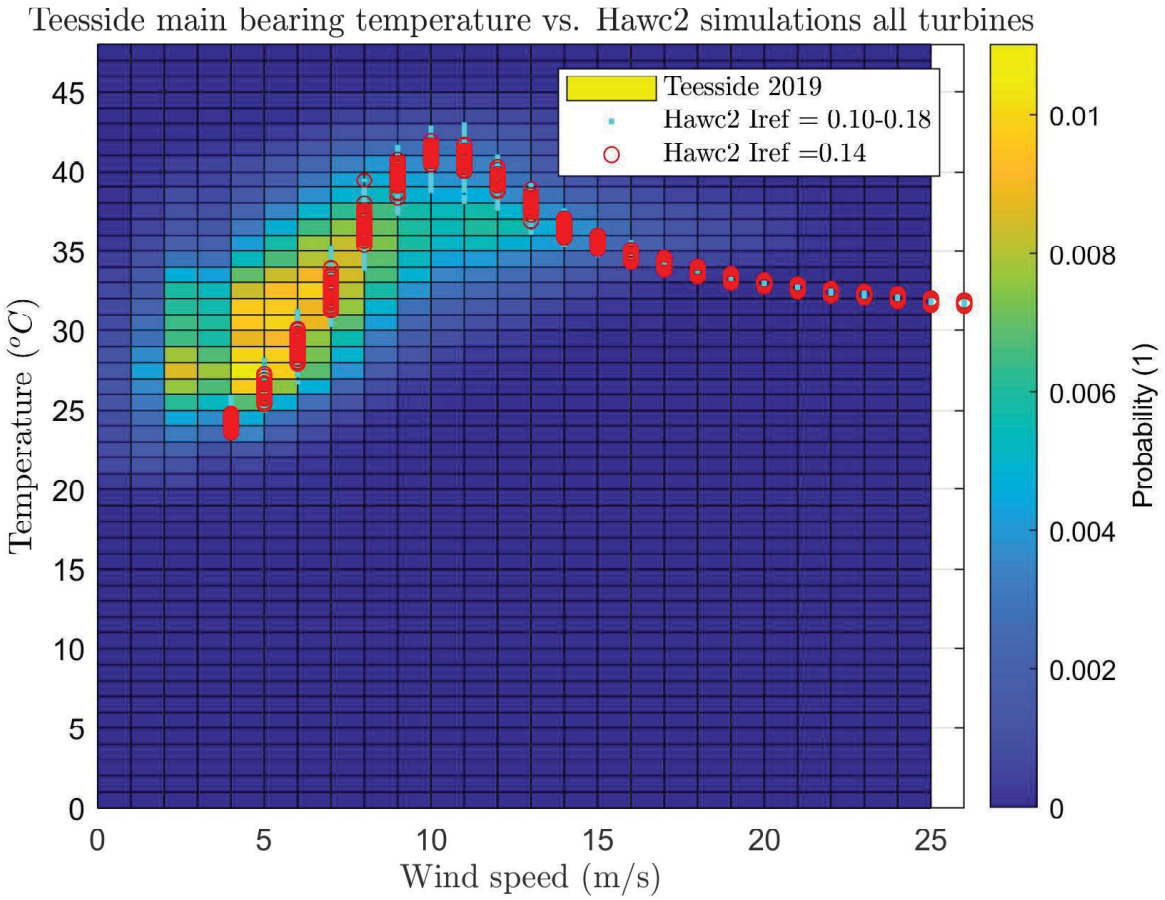

Figure 4.16: Combined correlation between the main bearing temperature and the wind speed of the measured SCADA data and the prediction of the aeroelastic simulations for all 27 turbines of the Teesside wind farm in 2019.

4.2 Comparison of simulated aeroelastic thrust curve and Teesside turbine strain gauge signals

The main input signal for the main bearing lifetime model of the Hiperwind work is the thrust force on the turbine rotor as obtained from aeroelastic simulation of the SWT 2.3 - 93 turbines of Teesside. Thus if the simulated thrust forces are wrong then the lifetime prediction will also be inaccurate. The simulation-based rotor thrust predictions will here be validated by 1 month of strain gauge measurements taken in 2019 at the transition piece of the WT13 turbine of the Teesside wind farm.

Figure 4.17 shows the transition piece between the monopile foundation and the tower as a simple schematic as well as the load sensors setup, formed by 3-pairs of opposed strain gauges. The $\gamma(t)$ is the time-varying yaw angle while $\Delta\theta$ is the difference between the coordinate system of the SCADA and the strain gauge positions.

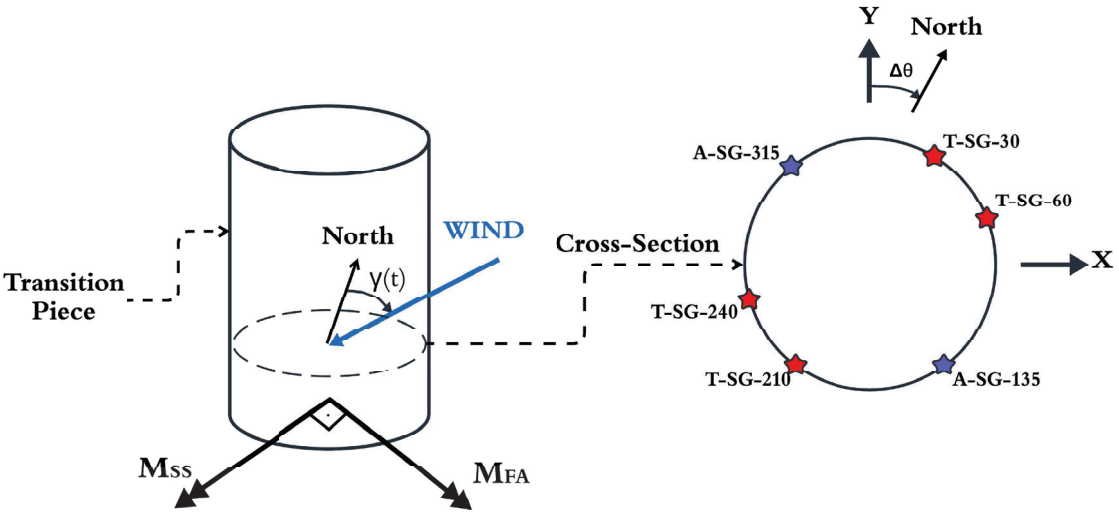

Figure 4.17: Schematic of the Teesside WT13 transition piece, containing the cross-section view in which the six strain gauges are installed. The $\gamma(t)$ represents the yaw angle and the $\Delta\theta$ the difference between the 0-degree directions of the stationary (strain gauges setup) and the moving nacelle coordinate systems.

Three resultant bending strains (ε_{BM}) can be calculated from the 6 individual sensors while considering only the aerodynamic and canceling the purely compressive loads as shown below

$$\begin{aligned} \varepsilon_{BM_{AG-45}} &= \frac{\varepsilon_{A-SG-315} - \varepsilon_{A-SG-315}}{2} \\ \varepsilon_{BM_{TG1-300}} &= \frac{\varepsilon_{T-SG-210} - \varepsilon_{T-SG-30}}{2} \\ \varepsilon_{BM_{TG2-330}} &= \frac{\varepsilon_{T-SG-240} - \varepsilon_{T-SG-60}}{2} \end{aligned} \tag{4.5}$$

In order to compare the downwind (Mx) and crosswind (My) HAWC2 simulated bending moments at the transition piece of the monopile with the measured Fore-Aft (FA) and Side-Side (SS) bending moments, post-processing procedures were necessary to address three issues:

- The three calculated bending strains from the 3-pair strain gauges would result in non-perpendicular bending moments.
- The offset angle $\Delta\theta$ is unknown.
- The zero point offset of the strain gauges is also unknown (not calibrated)

First in order to retrieve the perpendicular bending strains, $\varepsilon_{BM_{TG1-300}}$ and $\varepsilon_{BM_{TG2-330}}$ are combined into a resultant $\varepsilon_{BM_{TG-315}}$ averaging the previous two channels. In this way, two perpendicular bending strain $\varepsilon_{BM_{TG-315}}$ and $\varepsilon_{BM_{AG-45}}$ was obtained.

$$\epsilon_{BM_{TG-315}} = \frac{\epsilon_{BM_{TG1-300}} + \epsilon_{BM_{TG2-330}}}{2} \tag{4.6}$$

Then to estimate the $\Delta\theta$, the 10-min average bending strains are visualized versus the yaw angle $\gamma(t)$. Is it expected that the highest mean bending moment in $\varepsilon_{BM_{TG-315}}$ is measured at $225°$ and the lowest at $45°$, so basically when the wind is facing the same direction as the correspondent strain gauges. However, as seen in Figure 4.18, the peak of the T-SG bending

moment is around $225°$ (same for the zero-point on the A-SG bending moment). In this way, $\Delta\theta$ is estimated to be around $20°$, and should be accounted for ($\gamma_{cor}(t)$) when rotating the bending strains into the rotating coordinate system of the nacelle (FA and SS bending strain).

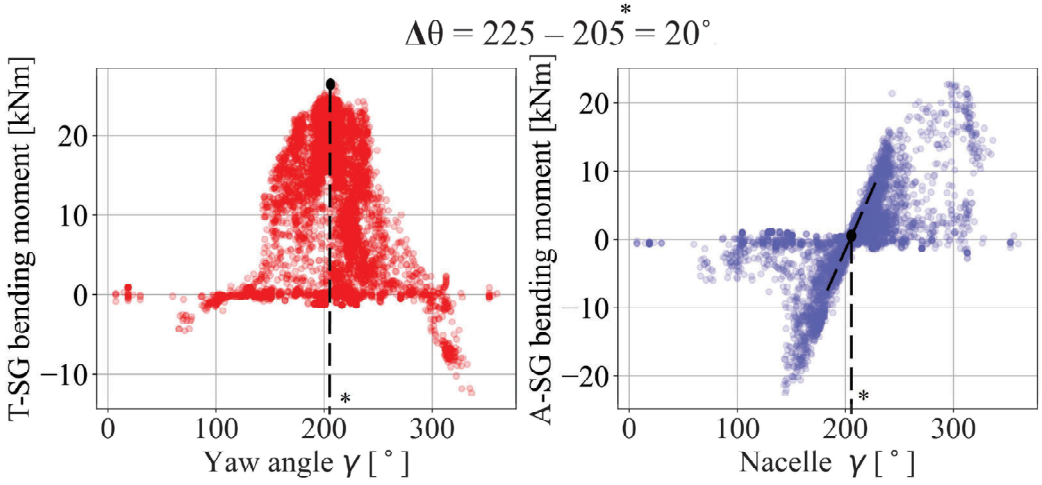

Figure 4.18: Resultant T-SG bending moment from combined T-SG strain gauges and A-SG bending moment from combined A-SG strain gauges plotted against yaw angle in 10-min average values. The difference between coordinate systems $\Delta\theta$ of the yaw angle $\gamma(t)$ and strain gauges setup was found to be 20°.

$$\gamma_{cor}(t) = \gamma(t) + \Delta\theta \tag{4.7}$$

The offset of the bending strain signals was estimated by manually adjusting the thrust curve of each channel separately ($\varepsilon_{BM_{TG-315}}$ and $\varepsilon_{BM_{AG-45}}$) so to present zero bending for low wind speeds (below cut-in). This method is not precise, but a more robust calibration was unfeasible as only 10-min SCADA is available Faria et al. (2024).

Once two perpendicular and approximately calibrated bending strains were retrieved, the latter were rotated from the strain gauges setup coordinate system to the rotating nacelle coordinate system by multiplying them with a rotation matrix, aligning them with the new coordinate axes, as shown in the following equation:

$$\begin{pmatrix} \varepsilon_{BM_{FA}} \\ \varepsilon_{BM_{SS}} \end{pmatrix} = \begin{pmatrix} \sin(45 - \gamma_{cor}(t)) & -\cos(45 - \gamma_{cor}(t)) \\ \cos(45 - \gamma_{cor}(t)) & \sin(45 - \gamma_{cor}(t)) \end{pmatrix} \begin{pmatrix} \varepsilon_{BM_{AG-45}} \\ \varepsilon_{BM_{TG-315}} \end{pmatrix} \tag{4.8}$$

Finally, the comparison between measurements and simulated responses are performed using 10-min average bending moments as functions of wind speed. Equation 4.9 is used to convert the bending strain into bending moment.

$$M_{bending} = \frac{\varepsilon_{BM} * E * I_r}{R_i} \tag{4.9}$$

where E is the material Young's modulus, R_i is the internal radius of the cross-section and I_r is the second moment of area of the cross-section (hollow cylinder) calculated as $I_r = \pi/4 *$

$(R_e^4 - R_i^4)$, where R_e is the external radius. The dimensions of the transition piece have been estimated to be a diameter of $D_{transitionpiece} = 4.251m$, a steel thickness of $t_{steel,TP} = 0.085m$ and the youngs modulus is assumed to be $E = 210GPa$.

Figure 4.19 presents the comparison between measured and simulated thrust curve (measured FA and simulated Mx downwind) and crosswind response (measured SS and simulated My crosswind). The simulated loads in both directions are higher than the measured, mainly for rated and above rated wind speeds. This difference could be justified by poor calibration of the strain gauges and manual coordinate systems adjustments, but could also highlight an overestimation of the loads and, potentially, of the consumed bearings lifetime in the simulated framework. Secondly the height position of the strain gauges are not completely accurate in the aeroelastic simulation, because the 30000 simulations were performed before receiving the information about the exact location of the strain gauges. The difference between the peak thrust values are approximately

$$\frac{M_{aero} - M_{measured}}{M_{measured}} = \frac{28MNm - 24MNm}{24MNm} \approx 17\% \tag{4.10}$$

which is similar to the combined uncertainty of the parameters entering the aeroelastic simulation and the transformation from strain to bending moment. Thus within the expected uncertainty then the simulated aeroelastic thrust loads are close to the measured bending moments of the Teesside turbines and with a difference in the order of 17 %. This discrepancy could probably be lowered further, but resource constraints did not allow for further optimization. However, the thrust force of the aeroelastic simulations have been validated to be realistic and properly capturing the dependence between wind speed and thrust force as expressed in the data.

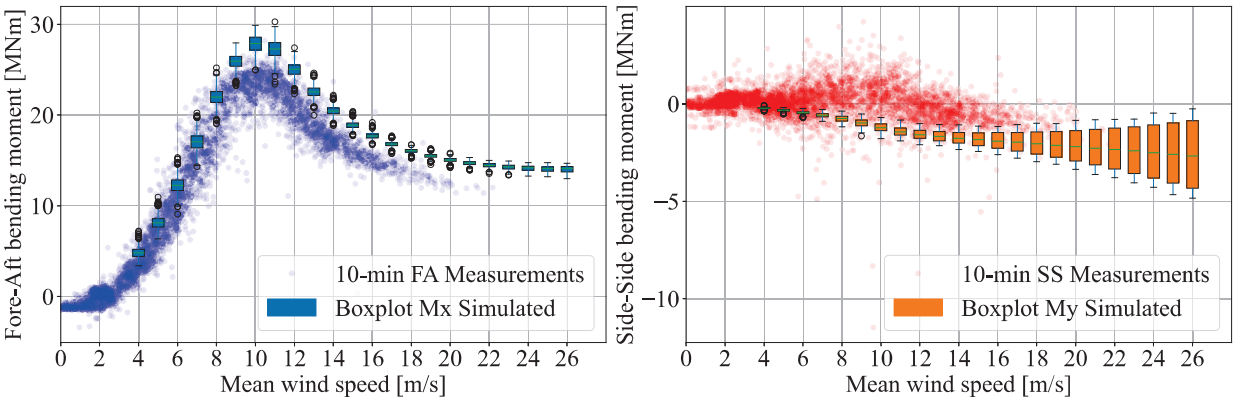

Figure 4.19: Comparision between Teesside WT13 monthly measurement campaign and HAWC2 simulation responses. Left: Fore-Aft (FA) transition piece bending moment. Right: Side-Side (SS) transition piece bending moment. Note: HAWC2 10-min average results have been combined into box-plots for the sake of simplicity.

4.3 Comparison of predicted main bearing life with Teesside failure statistics

The failure statistics of the Teesside offshore wind farm have recently been reviewed in a paper by Moros et. al. Moros et al. (2024) and presented at the Torque 2024 conference. Figure 4.20

is showing the failure statistics of each wind turbine after 9 year of operation of the Teesside wind farm and 3 large maintenance costs are observed for WT10, WT13 and WT19, where preventive gearbox replacements have been performed.

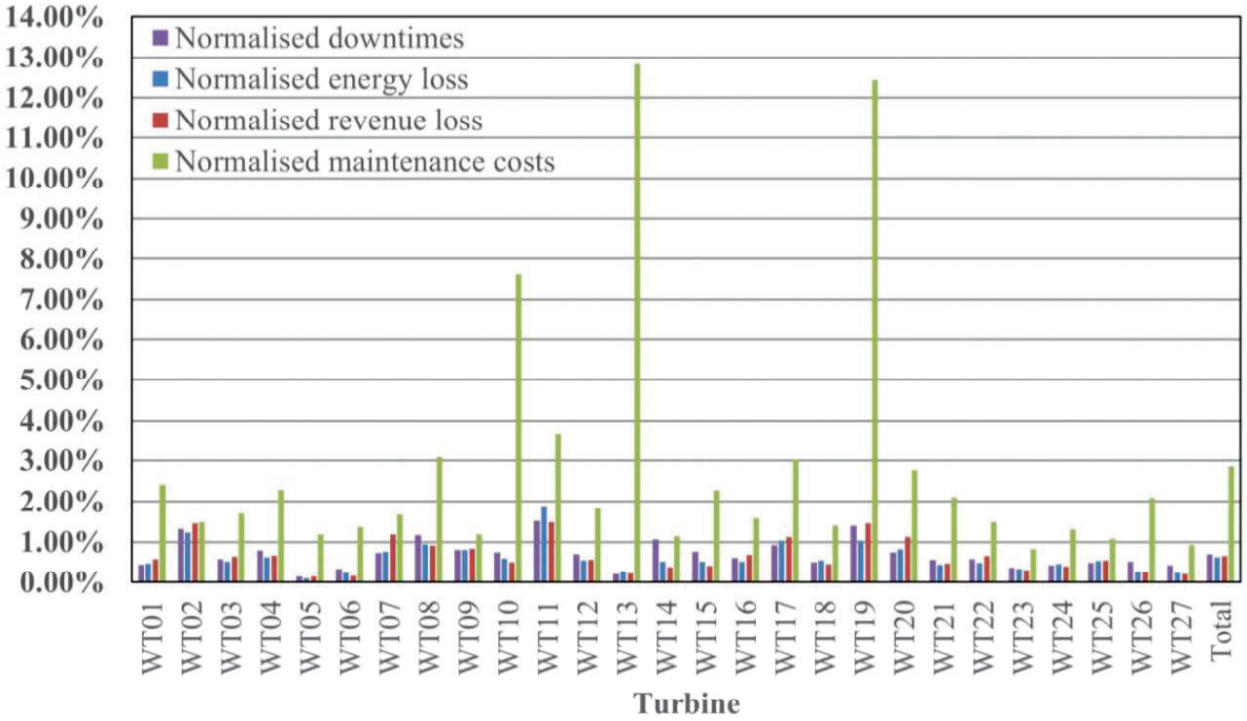

Figure 4.20: Failure statistics of the Teesside offshore wind farm shown by the normalised downtime, energy loss, revenue loss and maintenance cost of each wind turbine denoted WT1-27. Reproduced from Moros et. al. Moros et al. (2024).

The breakdown of the Teesside turbine failures into the turbine components is shown in Figure 4.21. Here it is of course interesting to notice that there have been no problems with the main bearings in the first 9 years of operation. This is not too surprising, since the main bearing is considered a structural component of the turbine and is expected to have a lifetime similar to the design lifetime of the turbine. In the case of the Teesside offshore wind farm then the design lifetime of the turbines is 25 years according to IEC 61400-3 standard EIC (2019).

Finally, Figure 4.22 shows the failure rates of the main components of the Teesside turbines for the first 9 years of operation and it is interesting to compare the predicted failure rates of the main bearing with these numbers.

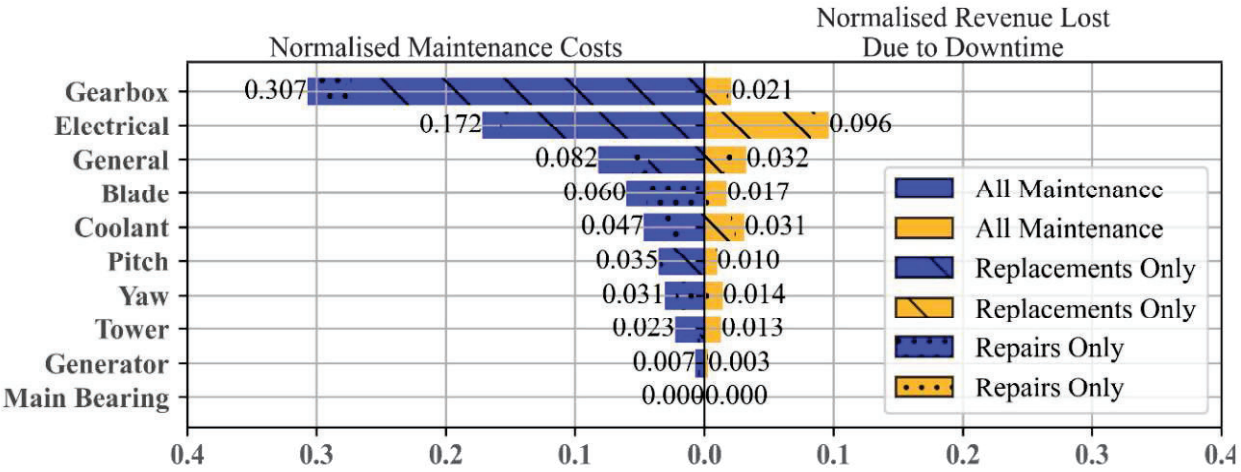

Figure 4.21: Failure statistics of the Teesside offshore wind farm broken down by components after 9 years of operation. Reproduced from Moros et. al. Moros et al. (2024).

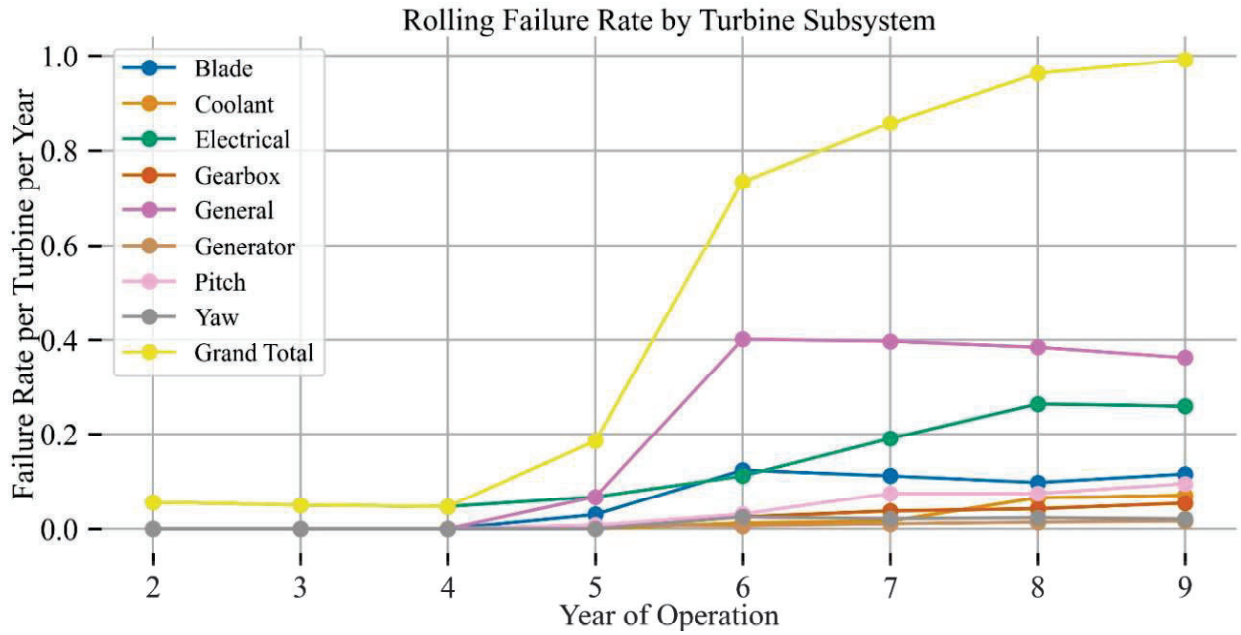

Figure 4.22: Rolling Failure rates of the main components of the Teesside offshore wind farm after 9 years of operation. Reproduced from Moros et. al. Moros et al. (2024).

5 Discussions

The validation of the correlations between the main bearing temperature and the wind speed of the Teesside wind farm and the prediction from the aeroelastic lifetime model is a major result because the method can be used to predict the temperature limits of the main bearings of wind turbines when evaluating their expected lifetime. There are, however, several limitations of the methods, which are related to the simple formulation of the thermal model, which does not take the heat capacity of the steel into account. A more elaborate model should probably take the form

$$mc_p \frac{\partial T}{\partial t} = \dot{Q}_{in} - \dot{Q}_{out} \tag{5.1}$$

where T is the temperature of the main bearing, t is time, m is the effective mass of the main bearing and shaft, c_p is the specific heat capacity of the steel of the main bearing and shaft, $\dot{Q}_{in}$ is the inflow of heat and $\dot{Q}_{in}$ is the outflow of heat caused by cooling. The simple model assumes thermal equilibrium whereby $\frac{\partial T}{\partial t} = 0$ and the main bearing temperature is found from matching the heat input with the cooling, $\dot{Q}_{in} = \dot{Q}_{out}$. In simple terms then the simple thermal model assumes that thermal equilibrium is obtained infinitely fast and that the temperature of the main bearing will just follow the heat inflow. In reality, there will be a time delay between the input heat being increased to maximum and until the main bearing temperature also reaches the maximum. This effect can probably explain why the correlation between the main bearing temperature and the wind speed observed for the Teesside wind farm as shown in Figure 4.16 is positioned above the curve obtained from the aeroelastic simulations. The "time delay" effect will cause the real main bearing temperature to be closer to the average temperature of the curve when the wind speed is below the rated wind speed of the turbine. Secondly this delay effect could also explain why the peak around rated wind speed is not clearly observed in the measured main bearing temperature map. It should however be noted that the probability map of the main bearing temperature of the Teesside turbines in Figure 4.16 contains a weighting based on the Weibull wind speed probability distribution, which has an average annual wind speed of $v_{ave} = 7.1m/s$ for Teesside and therefore it is only the position of the aeroealstic relationship curve that should compared to the temperature map, and not the probability.

One can pose the question if the aeroelastic main bearing life time model could benefit from a more advanced thermal model in the form of eq.(5.1 and the answer is most likely no, because the weighting of the aeroelastic time series is done with the annual Weibull distribution of the wind speed probabilities and this holds no information about the time correlation between the different wind speeds. Thus with the current implementation one will not be able to represent the thermal hysteresis due to the heat capacity of the main bearing and shaft. However, what is recommended as future work is to implement a monthly resolved Weibull wind speed distribution in the evaluation of the aeroelastic simulations, because this will be able to describe the seasonal change of the ambient temperature as observed in Figure 4.8 and also the slight increase of temperatures during the summer period. Secondly, it is expected that the average wind speed v_{ave} is showing a seasonal change as reported by the Global Wind Atlas and since the main bearing life consumption is mainly related to the peak of the turbine thrust curve then one could expect to see a seasonal difference in the resulting lifetime consumption over a year.

The physics-based main bearing life model of Hiperwind holds the potential to study the effect of FAG 230/800 main bearings in SWT 2.3 - 93 turbines not operating under optimal conditions, where the grease is contaminated or when a bearing is showing signatures of coming failures. The effect of contaminated grease is that the cleanliness factor e_c can decrease and, in principle, approach zero, whereby the main bearing life will degrade very fast. In this study we have focused only on the clean grease case, since this represents the ideal operation and thereby the most optimistic guess on the main bearing lifetime. It is very easy to argue for a much shorter main bearing life if the grease contamination is increased or if the temperature of the main bearing is increasing above the predicted curve of Figure 4.16. If the main bearing starts to degrade, then metal debris will accumulate in the grease, and secondly, the surface roughness of the metal parts of the bearing will increase. An expected result will be an increased friction

torque of the main bearing and therefore an increase above "normal main bearing temperature" due to additional friction heat dissipation. This is often utilized in the condition monitoring systems of main bearings of wind turbines to create a traffic light indicator showing a green, yellow and red signal depending on the maximum main bearing temperature. In the case of the Teesside wind farm there have been no main bearing replacements yet, and there is therefore no SCADA record of the main bearing temperature increase during the evolution of a main bearing failing. It is recommended to compare the physics-based main bearing life model to such a future measurement from a failing main bearing and investigate if the grease contamination factor can be determined from the model and then compared with real contamination measurements of the grease coming from the bearing. The advantage of this could be an online condition monitoring indicator of the grease contamination to supplement the usual yearly or bi-yearly test of the main bearing grease of offshore wind turbines. Finally, it should be stated that the validation of the thrust curve with the measurements of the Teesside turbine WT13 has provided confidence that the model predictions are based on reasonable input parameters in terms of the thrust force of the SWT 2.3 - 93 turbine. It would have been interesting to expand the analysis to more turbines of the Teesside wind farm, but resource limitations prevented this. Secondly, the proposal of introducing a monthly resolved main bearing life model could benefit from a monthly resolved analysis of the thrust forces, because that would provide a validation that the aeroelastic models is capable of replicating the seasonable fluctuations. An additional aspect to consider for the monthly resolved model would also be to be able to describe the seasonal variation of the wind direction of the wind farm, because the turbulence is expected to be different when coming from land and from sea as discussed in Hiperwind deliverable D5.4 (Abrahamsen et al., 2024).

6 Conclusions

The Hiperwind project has been working on validating a physics-based lifetime model of the FAG 230/800 main bearing of a SWT 2.3 - 93 turbine in relation to the Teesside offshore wind farm in UK. Since the main bearing life model basically transfers the turbine thrust force into the axial load of the main bearing and finally into life, then the validation of the thrust forces of the aeroelastic simulation was obtained by comparing the simulated thrust force as a function of the wind speed with the bending moment of the transition piece of the Teesside WT13 turbine as obtained from strain gauges. The peak transition piece bending moment of the simulations was found to be about 17 % higher than the measured bending moments, which is within the expected range of uncertainties. The main validation of the physics-based life model was the comparison of the predicted main bearing temperature as a function of wind speed based on the aeroelastic simulation against the measured main bearing temperatures of the Teesside turbines in 2019. The physics-based model predicted the temperature span of the Teesside main bearings and this has given confidence that the estimated lifetime modification factor for system approach a_{iso} determined from the ISO 281 standard is approximately correct in the Hiperwind deliverable D5.4.

Acknowledgements

This work is a part of the HIghly advanced Probabilistic design and Enhanced Reliability methods for the high-value, cost-efficient offshore WIND (HIPERWIND) project, which has received

funding from the European Union's Horizon 2020 Research and Innovation Programme under Grant Agreement No. 101006689. The support is greatly appreciated. The authors gratefully acknowledge the computational and data resources provided on the Sophia HPC Cluster at the Technical University of Denmark, DOI: 10.57940/FAFC-6M81 .

References

A. B. Abrahamsen, S. Dou, A. Zeghidour, H. Berrabah, and C. Jacquet. Hiperwind deliverable report d5.4 - development and implementation of probabilistic and uncertainty quantification methods for reliability sensitivity analysis. Technical report, H2020 HIPERWIND project (Grant agreement No 101006689), 2024.

S. Bannister and R. McCall. Offshore decommissioning plan: Teesside offshore windfarm. Technical report, PPMS, 2011.

EIC. Iec 61400-1:2019 wind energy generation systems – part 1: Design requirements. Technical report, IEC, 2019.

B. R. Faria, N. Sadeghi, N. Dimitrov, A. Kolios, and A. B. Abrahamsen. Inclusion of low-frequency cycles on tower fatigue lifetime assessment through relevant environmental and operational conditions. *Journal of Physics: Conference Series*, 2767(4):042021, jun 2024. doi: 10.1088/1742-6596/2767/4/042021. URL https://dx.doi.org/10.1088/1742-6596/2767/4/042021.

ISO281. Rolling bearings – Dynamic load ratings and rating life: DS/ISO 281:2007. Technical report, ISO, 2007.

D. Moros, N. Berrabah, K. D. Searle, and I. G. Ashton. Maintenance & failure data analysis of an offshore wind farm. *Journal of Physics: Conference Series*, 2767(6):062006, jun 2024. doi: 10.1088/1742-6596/2767/6/062006. URL https://dx.doi.org/10.1088/1742-6596/2767/6/062006.

D. Remigius, B. Paz, Y. Liu, W. Remigius, and A. B. Abrahamsen. Hiperwind deliverable report d5.1 - component life models. Technical report, H2020 HIPERWIND project (Grant agreement No 101006689), 2023.

Schaeffler. Tpi 176 : Lubrication of rolling bearings. Technical report, Schaeffler Technologies, 2013.

TR1281-2. Rolling bearings – Explanatory notes on ISO 281 – Part 2: Modified rating life calculation, based on a systems approach to fatigue stresses : DS/ISO/TR 1281-2:2009. Technical report, ISO, 2009.